International Research Journal of Earth Sciences _____ ISSN 2321 – 2527
Vol. **7(1),** 29-56, January **(2019)** *Int. Res. J. Earth Sci.*

Influence of increased vertical resolution in RegCM4.5 on summer climate simulation over West Africa

Adeniyi M.O.
Department of Physics, University of Ibadan, Nigeria
mojisolaadeniyi@yahoo.com

Available online at: www.isca.in
Received 14th October 2018, revised 26th December 2018, accepted 15th January 2019

Abstract

The response of climate parameters to increase in vertical resolution based on a fixed horizontal resolution is simulated using RegCM4.5. Eighteen and 23 vertical levels are used for the simulation with 50 km x 50 km horizontal resolution in the LEV18 and LEV23 experiments, respectively. All other model parameters are the same except for the number of model vertical levels. Most of the climate parameters are better resolved in the higher resolution experiment. Air temperature is well captured by both vertical resolutions at upper and mid troposphere but LEV23 performs better at the surface. Simulations of omega pressure velocity from both resolutions have biases in terms of vertical and north-south extents and strength. Increased vertical resolution generally improves the simulated climate and makes it more realistic.

Keywords: Vertical resolution, regional climate, RegCM4.5, precipitation, temperature, zonal wind.

Introduction

Realistic simulation of climate is necessary in climate studies to understand climate phenomena and variability. Regional Climate Models (RCMs) are particularly useful in downscaling future projected climate from Global Circulation Models (GCMs), based on coarse horizontal resolution in GCMs. The fine horizontal resolution in most RCMs refines the simulated output and makes them more realistic. Most simulations are done using predetermined vertical and horizontal resolutions[1-5]. Interest of modellers in terms of fine resolution has been on the use of improved horizontal resolution and testing of different resolutions in the vertical for improved simulation of climate and weather parameters[6-8]. The effect of changes in vertical resolution on climate in a few GCMs has been simulated with differing conclusion no significant effect on MJO simulation was reported with improved vertical resolution in ECHAM4 GCM[9]. A similar result of no significant improvement with increased vertical resolution was obtained when horizontal resolution of T30 was used for two different simulations with 19 and 39 vertical levels, respectively[10]. Also, improved simulation was found with ECHAM5 model on 31 vertical levels than 19 levels[11]. These findings lend support to the criterion of consistency between vertical and horizontal resolutions[12]. When the consistency criterion is satisfied, improvement in simulations is expected with increased vertical resolution. Improved MJO simulation was reported with improved vertical resolution in HadAM3. In addition, more realistic spectrum of cloud and water vapour was simlated[13,14]. Furthermore, improved simulation of response of North Pacific to ENSO forcing with increased number of vertical levels in HadAM3 was documented[15]. Comparison of two ECHAM4 simulations on 19 and 42 vertical levels over the tropical band also resulted in improved simulation[16]. A few RCM have been used for similar studies. The Fifth Generation Penn State/NCAR Mesoscale Model (MM5) which is a regional mesoscale model (MM5) was used for a similar study[17]. It was concluded that, increased vertical and horizontal resolutions improved simulation of heavy rainfall and surface air temperature. Version 3 of the Weather, Research and Forecasting model (WRF) was used to study the effect of increased vertical resolution (16-28 vertical levels) on the climate of West Africa and increased strength in circulation, vertical wind shear and amplitude of Africa Easterly Waves was found[18]. Version 3 of the RCM (RegCM3) of the International Centre for Theoretical Physics (ICTP) with 14, 18 and 23 levels was employed in studying the influence of increased resolution in the vertical, on the climate of China[19]. There is need to con the influence of increased vertical resolution in RegCM4. However, the version four of the regional climate model up to RegCM4.4 has always been run with 18 vertical layers based on the advice of the model developers at ICTP[20]. In this paper, the latest version of RegCM4 (RegCM4.5) was used with 18 and 23 vertical levels to con the influence of increased vertical levels on simulation of climate over West Africa.

Model setup: The RegCM4.5 was used for the simulations. Details of the design and performance of RegCM4 are well documented[20-22]. Similar experimental setup, in Adeniyi (2016)[23] is used for two dynamical experiments, except for the different vertical resolutions. Eighteen and 23 sigmal levels corresponding to the pressure levels shown in Figure-1 were used, respectively, for LEV18 and LEV23 experiments. The two different vertical resolutions are distinct at the surface, planetary boundary layer and mid-troposphere up to the upper troposphere. The distinction reduces towards the upper

troposphere and there is no distinction between the two vertical resolutions beyond 150 hPa. The domain of simulation for the two different experiments is shown in Figure-2 with topography from Global 30 Arc-Second Elevation topography dataset. The experiments were from 00 GMT 01 May to 00 GMT 01 September 2007 while the analysis starts from June leaving one month spin up against errors from persisting initial soil moisture properties.

Validation datasets: Simulated precipitation was validated with the use of observational precipitation datasets from Climate Research Unit (version 3.22) on 0.5x0.5 degree grid[24] and Global Precipitation Climatology Project (GPCP) daily, version 1DD V1.1 on 1 degree grid[24-27]. Outgoing Longwave Radiation (OLR) simulation was validated using the interpolated National Oceanic and Atmospheric Administration (NOAA) OLR satellite retrieved data[28]. Era Interim data of air temperature, cloud liquid water content omega, zonal (u) and meridional (v) wind at pressure levels were also used to validate the simulated air temperature, cloud liquid water u wind, v wind and omega. In addition, Era Interim skin temperature was used to validate simulated ground surface temperature.

Results and discussion

The domain of simulation is characterized by varied topography (Figure-2); most of the mountains are at the eastern part of the region. Among them are the mountains at Jos in central Nigeria, Cameroon, Niger, southern Algeria, northern Chad and Morocco. The western part of the simulation domain is majorly highlands such as the highlands at Mauritania, Ivory Coast and Mali. Low lands are sandwiched between the mountains and highlands mostly at the Western part of the domain.

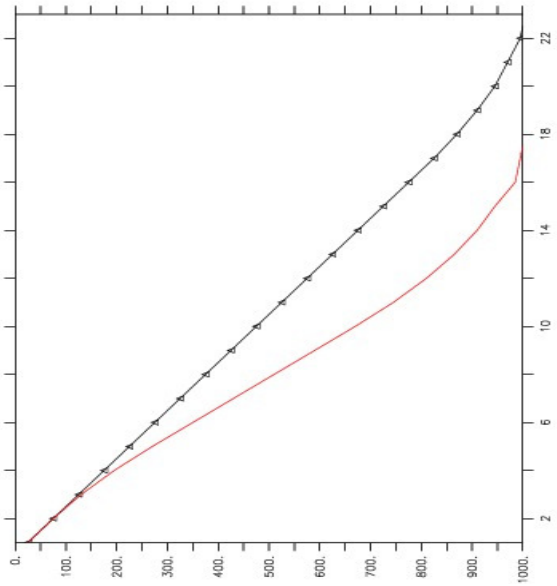

Figure-1: Pressure levels used in LEV18 and LEV23 experiments. The red curve represents LEV18, while the black curve with symbol represents LEV23".

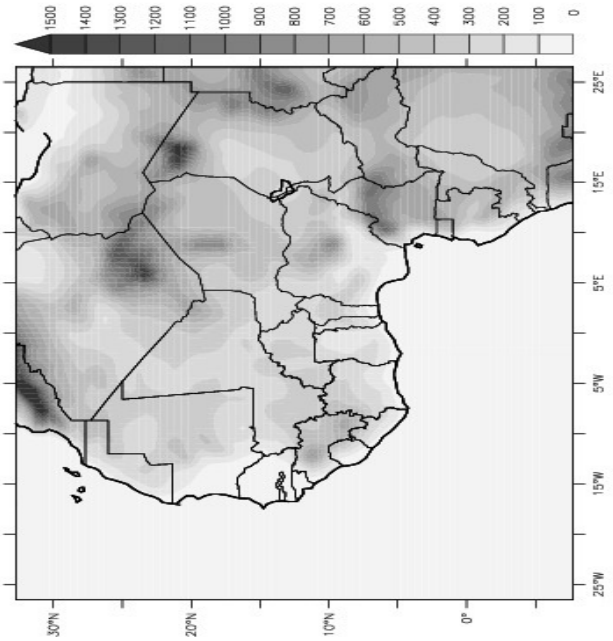

Figure-2: Topography of the simulation domain in meters above sea level.

Validation of simulated precipitation: Precipitation data in observation and simulation are compared in Figure-3. The CRU and GPCP observed precipitation have similar spatial pattern except for the mountain areas and the coast. While CRU has relatively higher precipitation at the coast, GPCP has higher precipitation at the mountain areas, for example at Jos in Nigeria (Figure-3a, b). Only GPCP has precipitation over ocean, so the two observed data cannot be compared over ocean. At the ocean and coast LEV18 and LEV23 overestimate precipitation. The spatial extent of significant simulated rainfall is far lower than observed in LEV18 (Figure-3). LEV23 simulates better spatial rainfall extent and values comparable with observation over land. LEV18 overestimates rainfall excessively at latitude 5-10N; longitude 15-25W (Figure-3e) and underestimates precipitation in most of the other areas. LEV23 has better representation of precipitation.

Validation of simulated ground surface temperature: Figure-4 shows ground surface temperature from Era-Interim reanalysis and simulations. Era-Interim shows hotter northern Africa starting from the Sahel, with the hottest area within 10W to 5E and 15 to 30N. This depicts the Sahara Thermal Low (STL). LEV18 overestimates ground temperature at the south and underestimates it at the north such that the observed distinction between ground temperature at the north and south is not obvious in LEV18. The spatial extent of STL in LEV18 is also low with respect to Era-Interim (Figure-4b). In the same vein, LEV23 underestimates observed ground temperature at the north and overestimates it at the south but it simulates ground temperature closer to Era-Interim than LEV18. Figure-4d shows higher ground temperature simulated by LEV23 at the north (15-25N) and lower at the south with respect to LEV18.

Validation of simulated outgoing longwave radiation: Figure-5 shows observed and simulated Outgoing Longwave Radiation (OLR), deep convection (OLR<245 Wm^{-2}) is found at the southern countries while higher OLR are at the north in observed NOAA. Only the far southeastern area, central Nigeria, the ocean (5-10N) and the coast have simulated deep convection in LEV18 (Figure-5b). LEV23 shows extended spatial coverage of simulated deep convection than LEV18 (Figures-5b, c, d; Figure-3c, d, e). This explains the spatial coverage of simulated precipitation in both vertical resolutions since precipitation is mainly convective over the tropics[29].

Ratio of convective precipitation to the simulated total precipitation in LEV18 and LEV23 experiments is shown in Figure-6. While LEV18 shows scattered substantial proportion of simulated convective precipitation, LEV23 has extended spatial spread of substantial proportion of convective precipitation below 15°N. LEV18 simulates little or no convective precipitation over land beyond 15°N. This is in support of the general simulation of more convective precipitation by higher vertical resolution experiment in most part of the tropics by ECHAM4 model[16]. The two vertical resolutions simulate the least proportion of convective precipitation at the Atlantic Ocean between 18-30°N and 20-15°W.

Validation of simulated cloud water content: Figure-7 shows observed and simulated zonal average of Cloud Water Content (CWC). It is documented that vertical resolution affects CWC and it is better represented by high resolution[13,16]. Era Interim (Figure-7a) shows resolved CWC up to the mid-troposphere (500 hPa). LEV18 does not resolve CWC beyond 600 hPa while LEV23 resolves it up to 500 hPa (Figure-7b, c).

Validation of simulated zonal wind: Figure-8 shows the vertical cross-section of zonal average of zonal wind. Africa Easterly Jet (AEJ) and Tropical Easterly Jet (TEJ) are shown at about 600 and 200 hPa, respectively in Era Interim and simulations. However, the AEJ is stronger in LEV23 than LEV18. LEV23 is closer to Era-Interim in terms of strength. While Era-Interim shows the AEJ core at 15N, LEV18 and LEV23 show the AEJ at 7.5°N.

Validation of simulated specific humidity: Figure-9 shows crossection of zonal average (-15 to 15°E) of specific humidity. LEV23 resolves the specific humidity better at the north than LEV18 with respect to Era-Interim. The vertical extent of specific humidity in LEV23 is also closer to Era-Interim than that in LEV18.

Validation of simulated air temperature: Figure-10 shows the cross section of zonal average of temperature. Temperature is well resolved at the upper- troposphere and mid-troposphere based on the two vertical resolutions. However, at the lower-troposphere temperature is better resolved by LEV23 than LEV18 with respect to Era-Interim.

Validation of simulated omega pressure velocity: Figure-11 shows ascent (omega pressure velocity) in Era-Interim and simulations. Ascent in Era-Interim at 5°N is captured by both resolutions but the north-south extent of the ascent is by far lower in simulations, the ascent is stronger in LEV23. Between 15°N and 25°N, the ascent in Era-Interim is also captured in simulations but stronger than Era-Interim and extends north-south than Era-Interim. Between 10-15°N at the lower troposphere, weak descent in Era-Interim is better captured by LEV23.

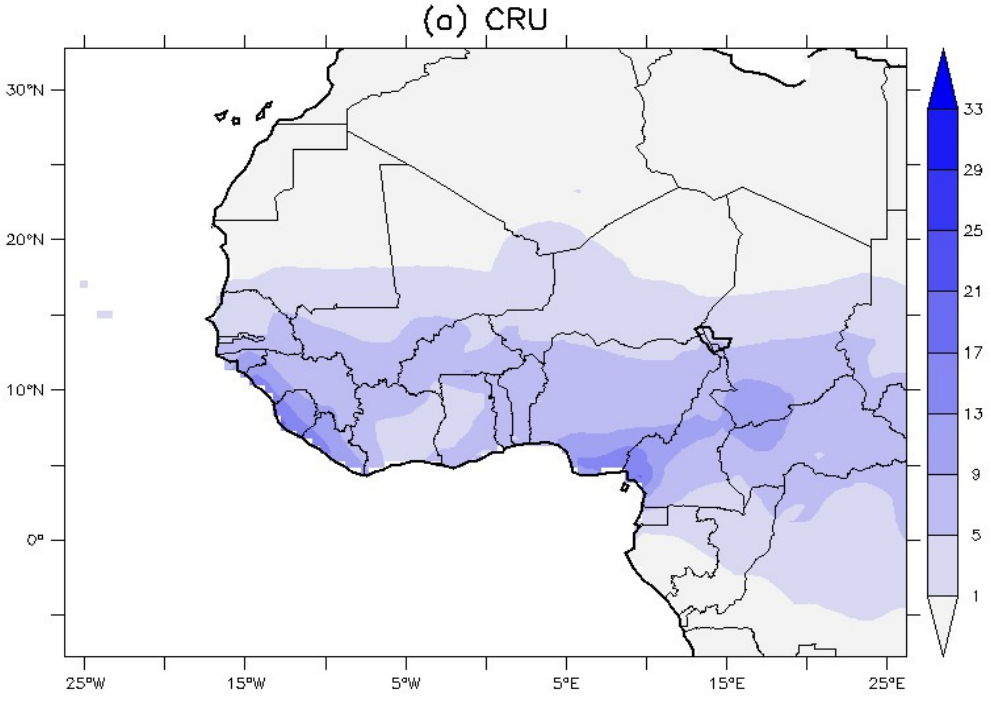

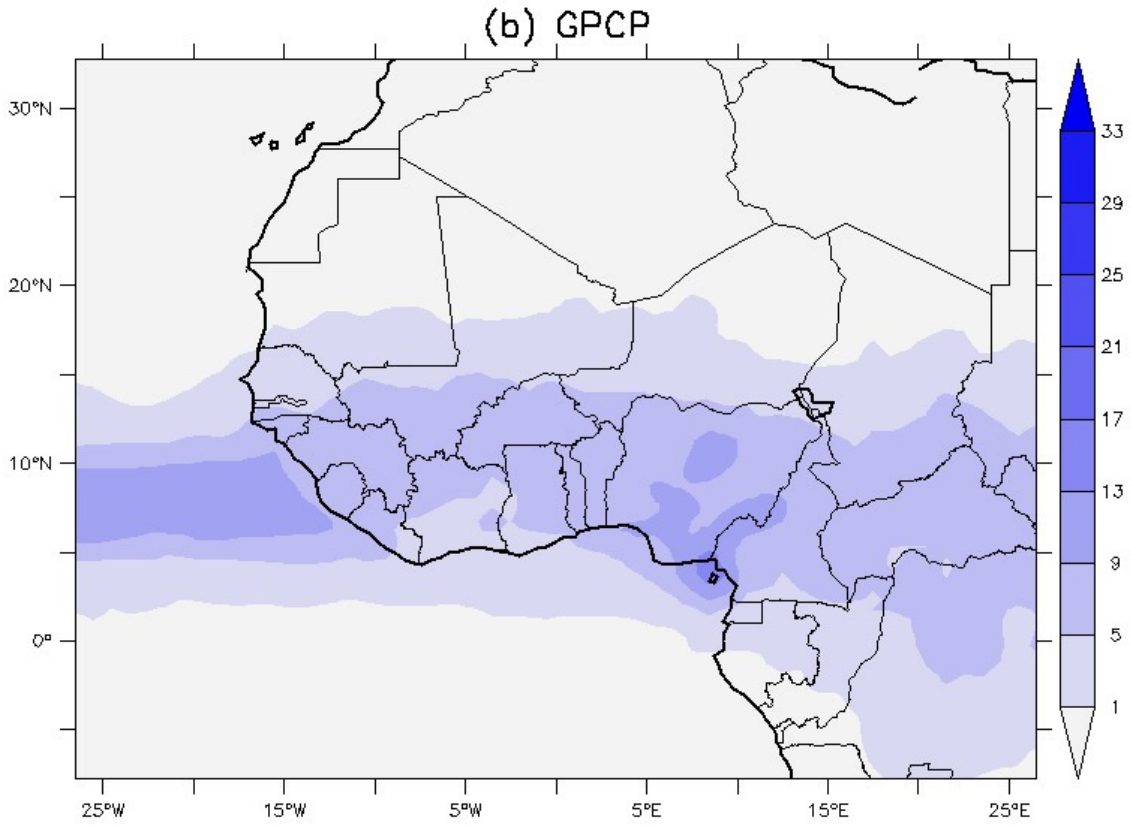
(b) GPCP
30°N
20°N
10°N
0°
25°W
15°W
5°W
5°E
15°E
25°E
33
29
25
21
17
13
9
5
1

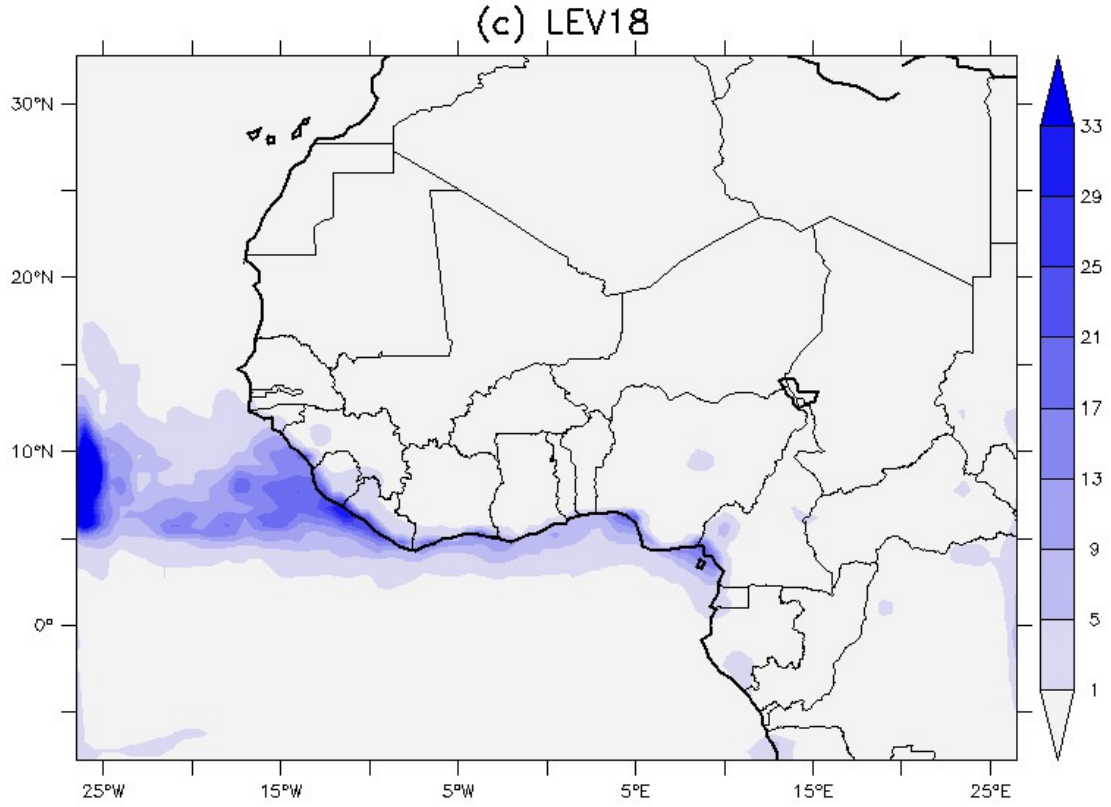
(c) LEV18
30°N
20°N
10°N
0°
25°W
15°W
5°W
5°E
15°E
25°E
33
29
25
21
17
13
9
5
1

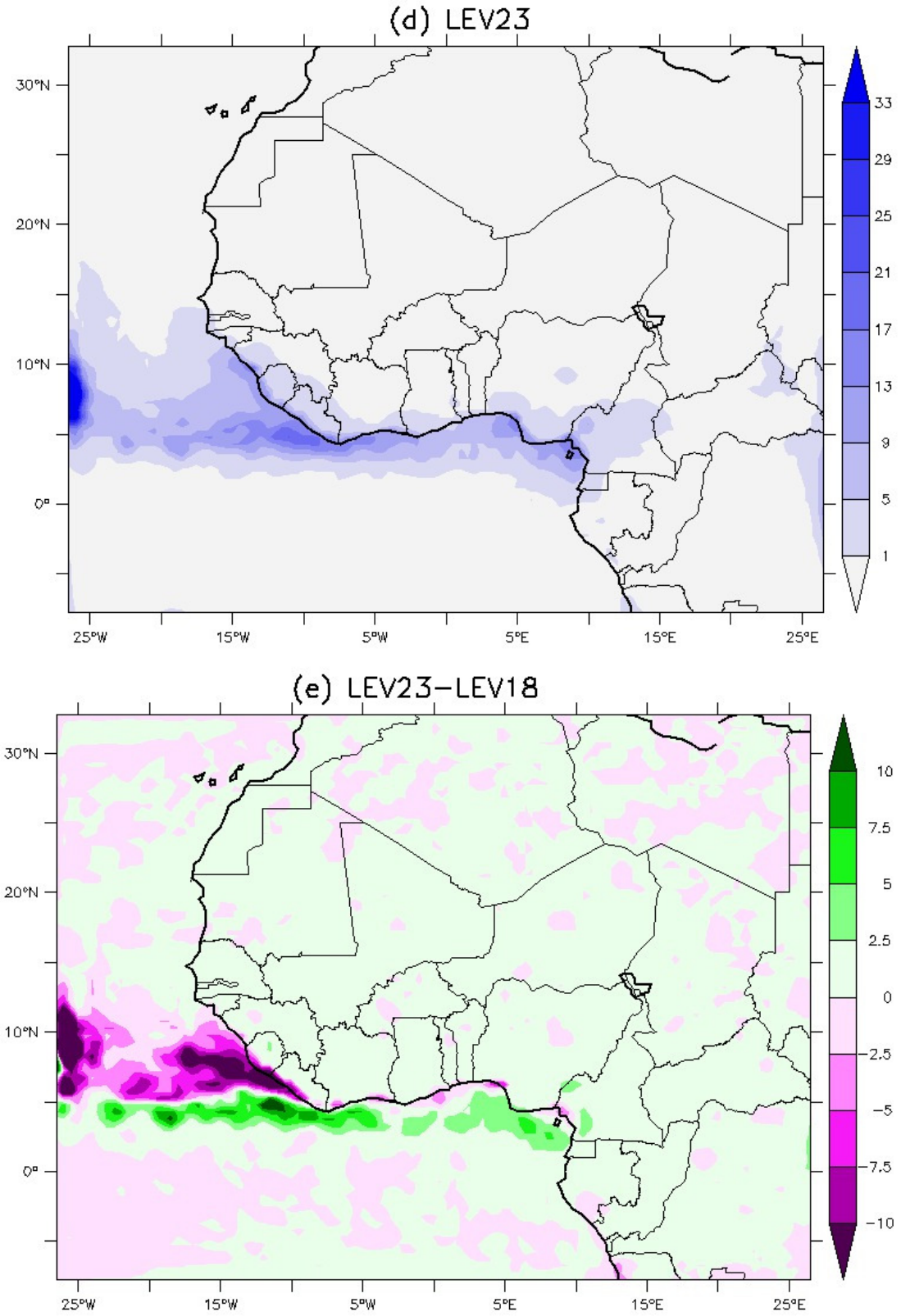

Figure-3: JJA 2007 seasonal precipitation ($mmday^{-1}$) in (a) CRU, (b) GPCP, (c) LEV18, (d) LEV23 and (e) difference between LEV23 and LEV18. LEV18 and LEV23 are simulations.

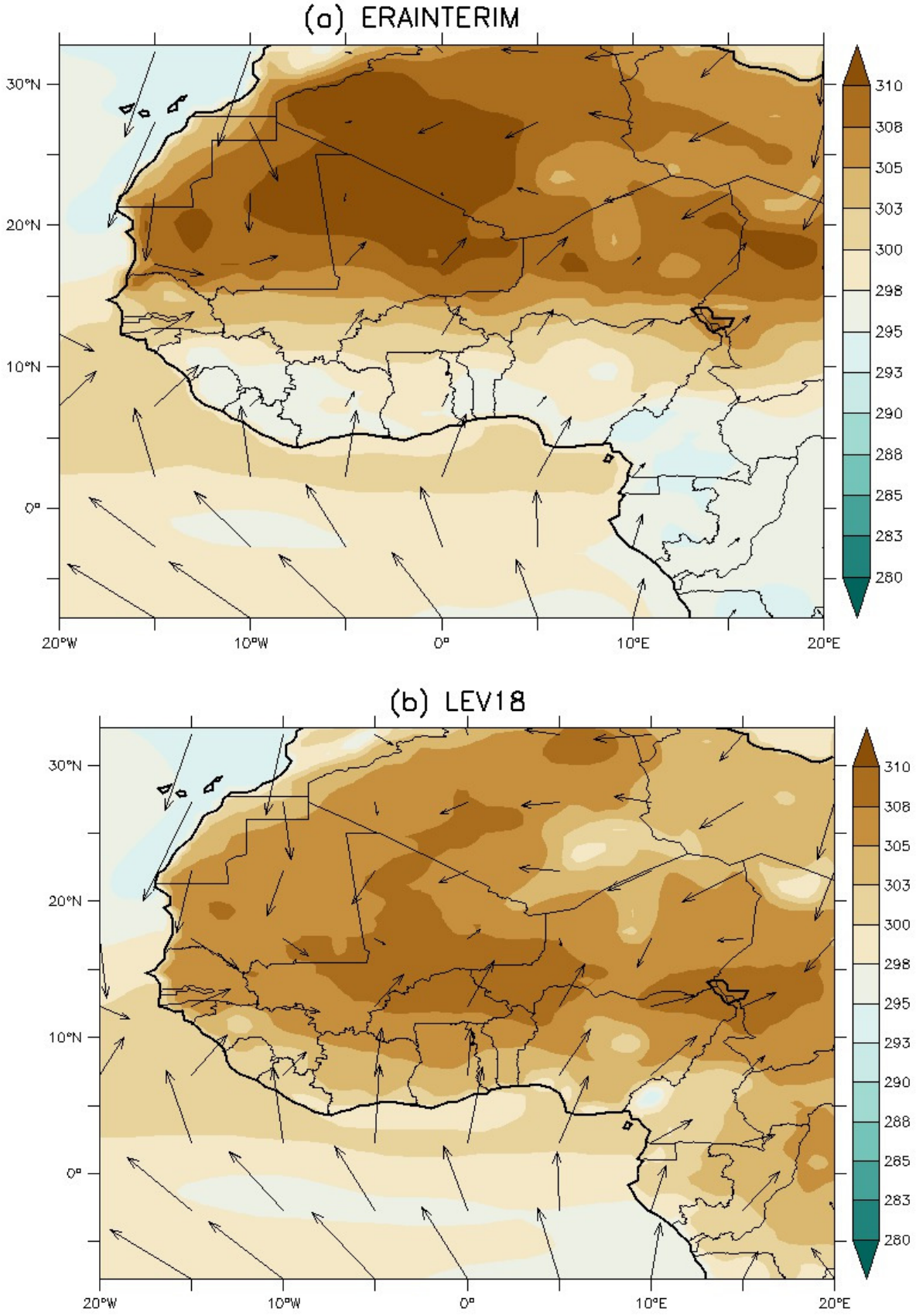
(a) ERAINTERIM
30°N
20°N
10°N
0°
20°W
10°W
0°
10°E
20°E
310
308
305
303
300
298
295
293
290
288
285
283
280
(b) LEV18
30°N
20°N
10°N
0°
20°W
10°W
0°
10°E
20°E
310
308
305
303
300
298
295
293
290
288
285
283
280

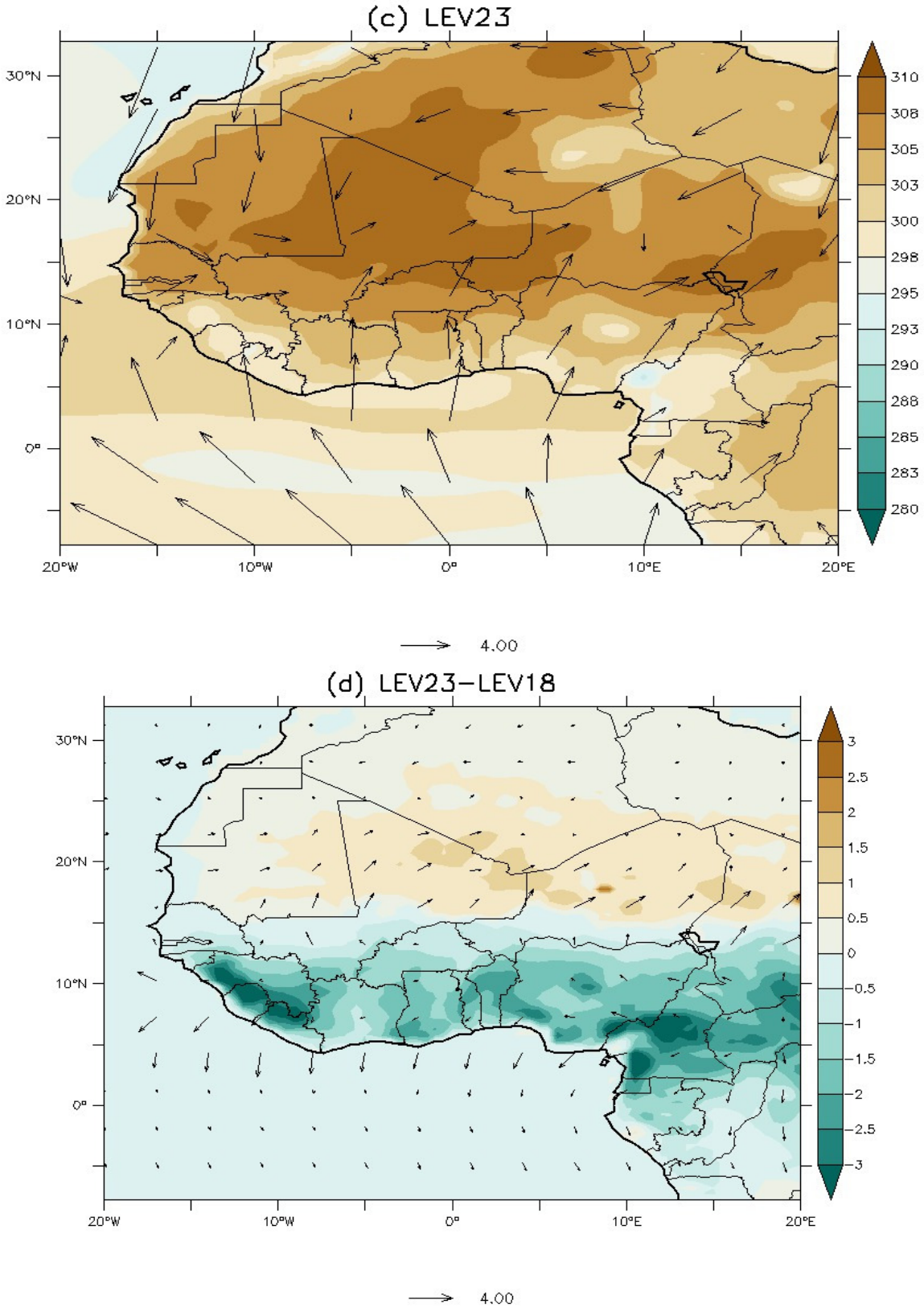

Figure-4: JJA 2007 ground surface temperature (K) in (a) Era-Interim, (b) LEV18 experiment, (c) LEV23 experiment and (d) difference between LEV23 and LEV18.

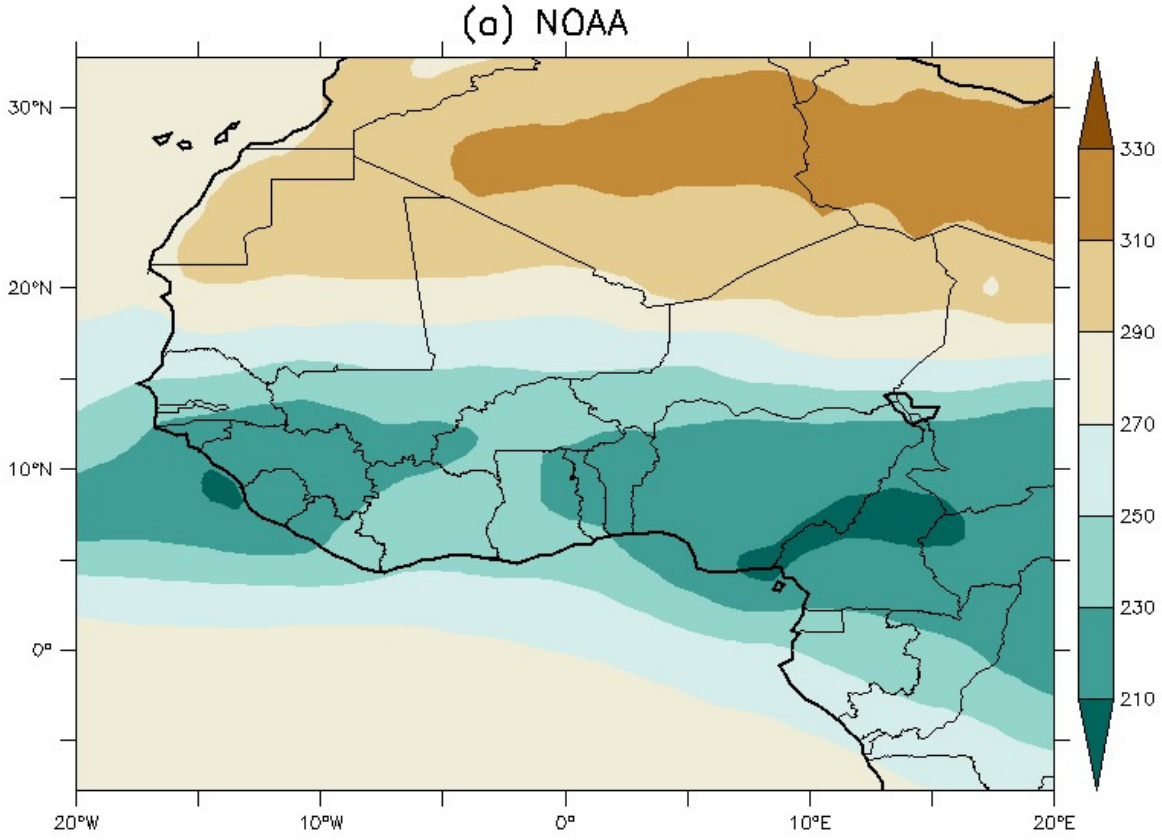
(a) NOAA
30°N
20°N
10°N
0°
20°W
10°W
0°
10°E
20°E
330
310
290
270
250
230
210

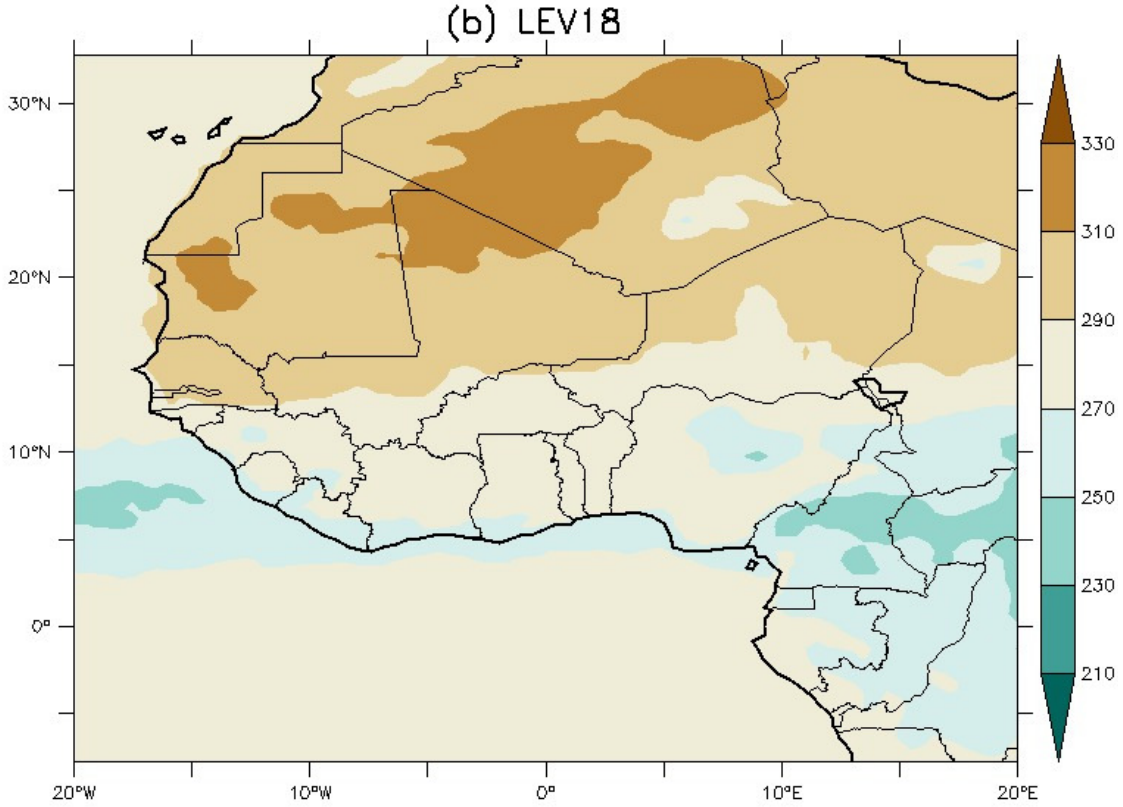
(b) LEV18
30°N
20°N
10°N
0°
20°W
10°W
0°
10°E
20°E
330
310
290
270
250
230
210

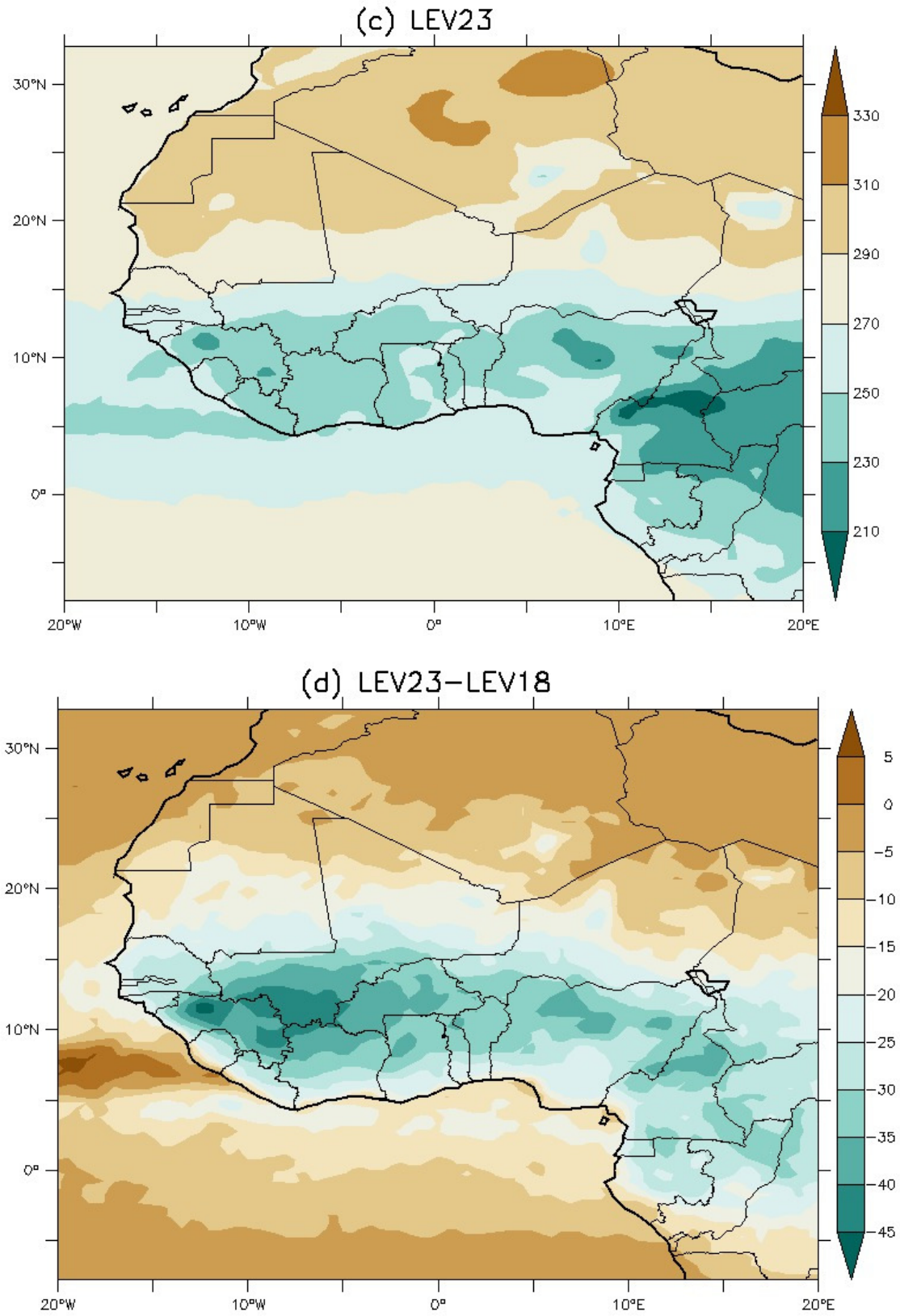

Figure-5: JJA Outgoing longwave radiation (Wm^{-2}) from (a) NOAA, (b) LEV 18 experiment, (c) LEV23 experiment and LEV23 experiment minus LEV18 experiment in 2007.

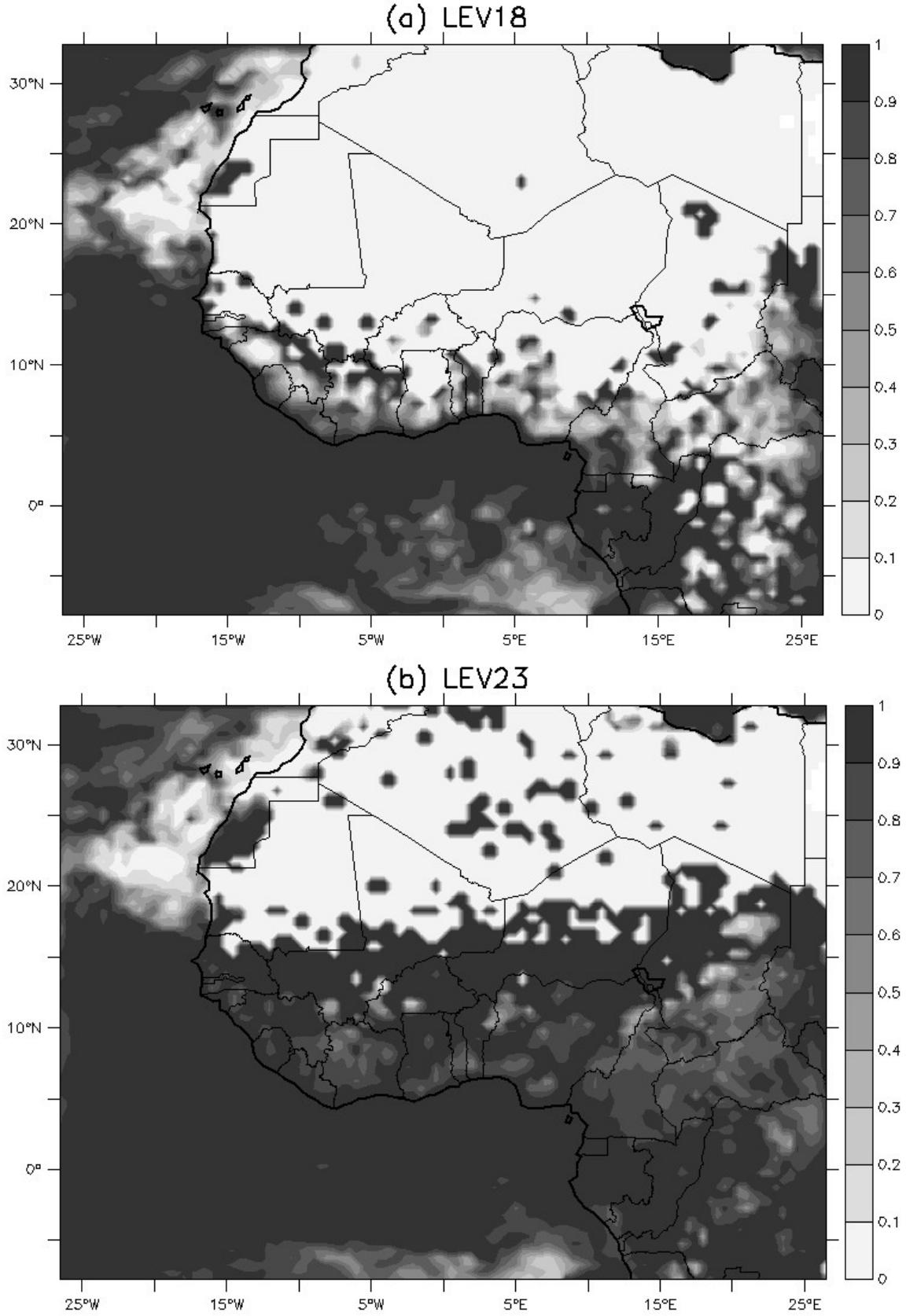

Figure-6: Proportion of convective precipitation from (a) LEV18 and (b) LEV23 experiments.

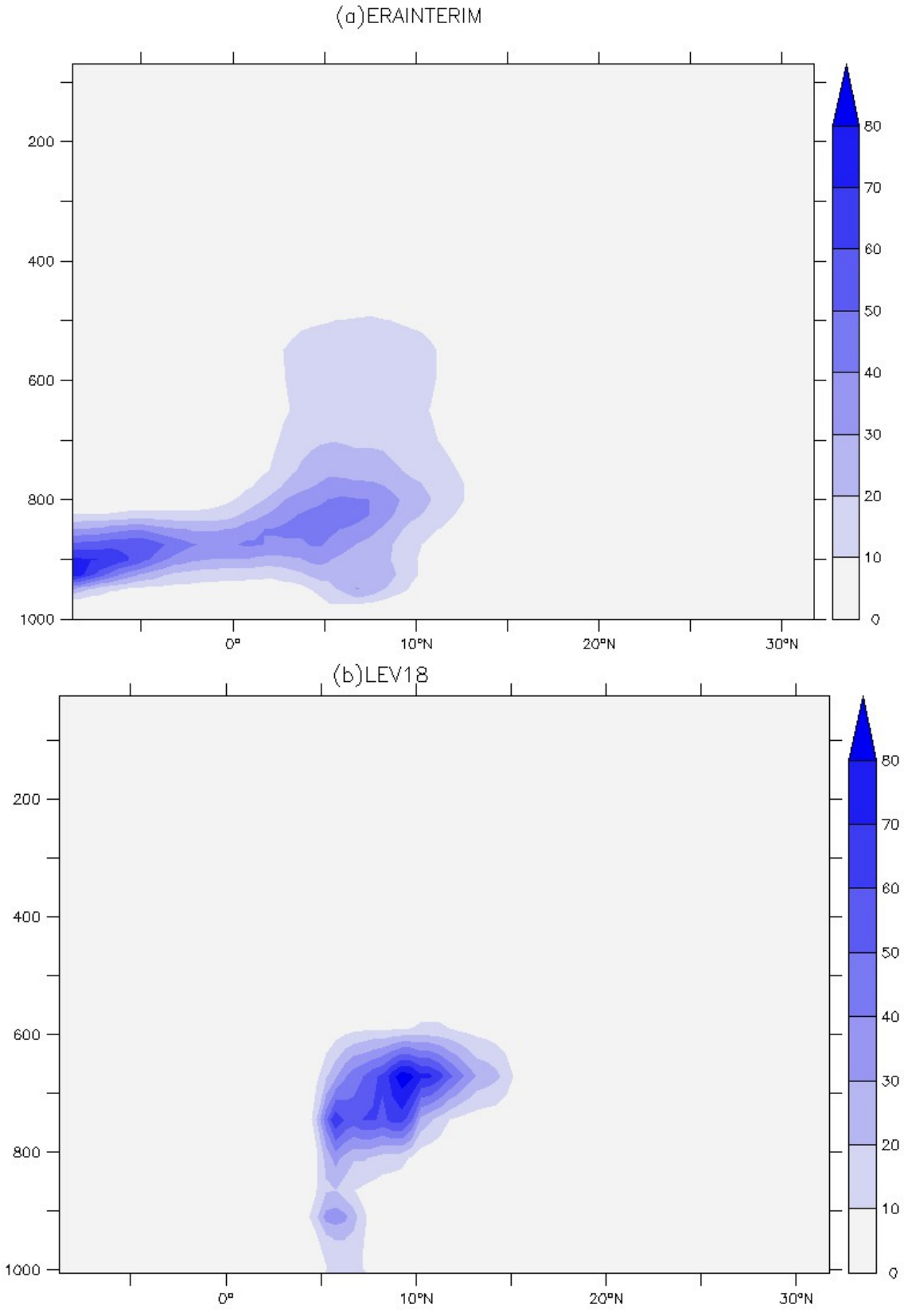
(a)ERAINTERIM
200
400
600
800
1000
0°
10°N
20°N
30°N
80
70
60
50
40
30
20
10
0
(b)LEV18
200
400
600
800
1000
0°
10°N
20°N
30°N
80
70
60
50
40
30
20
10
0

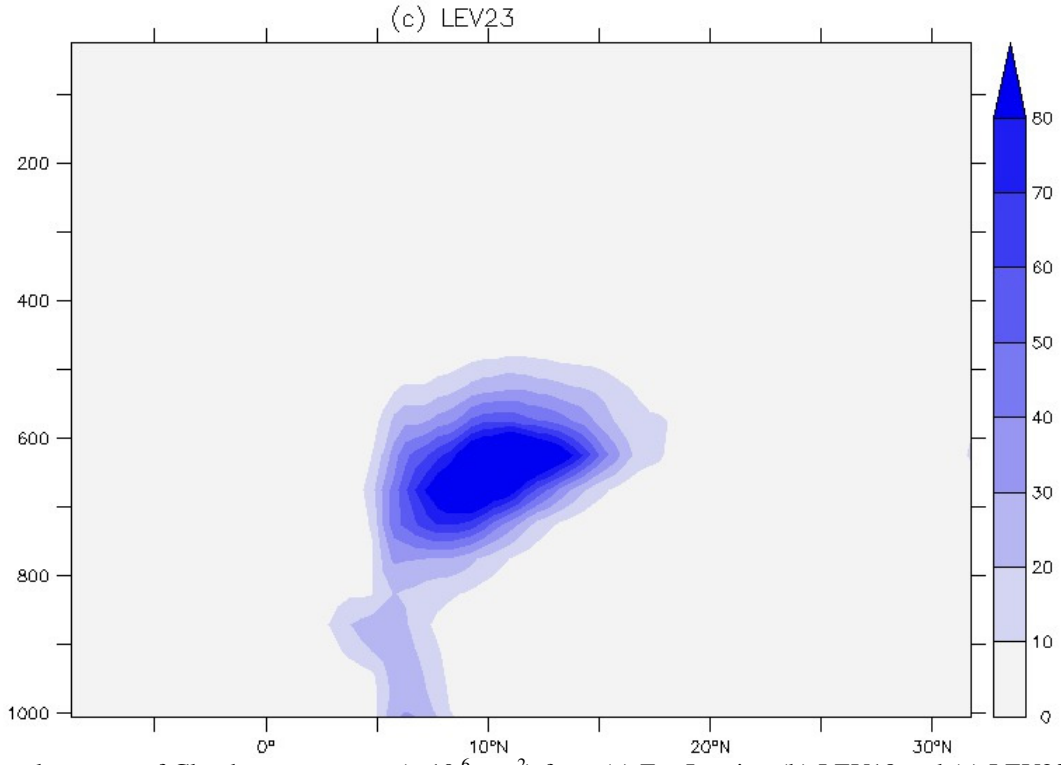

Figure-7: JJA zonal average of Cloud water content (x 10^{-6} gm^{-2}) from (a) Era-Interim, (b) LEV18 and (c) LEV23 experiments in 2007. The cloud water content is averaged over 15°W to 15°E.

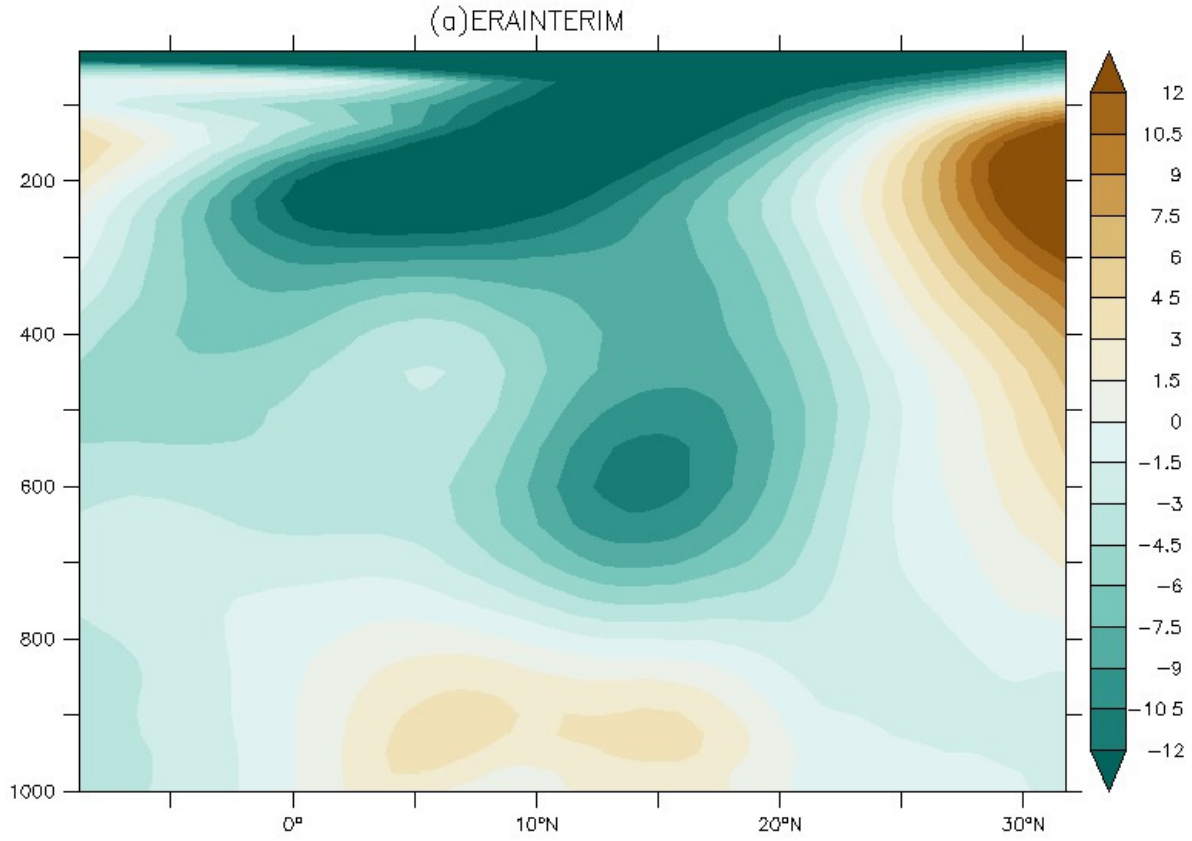

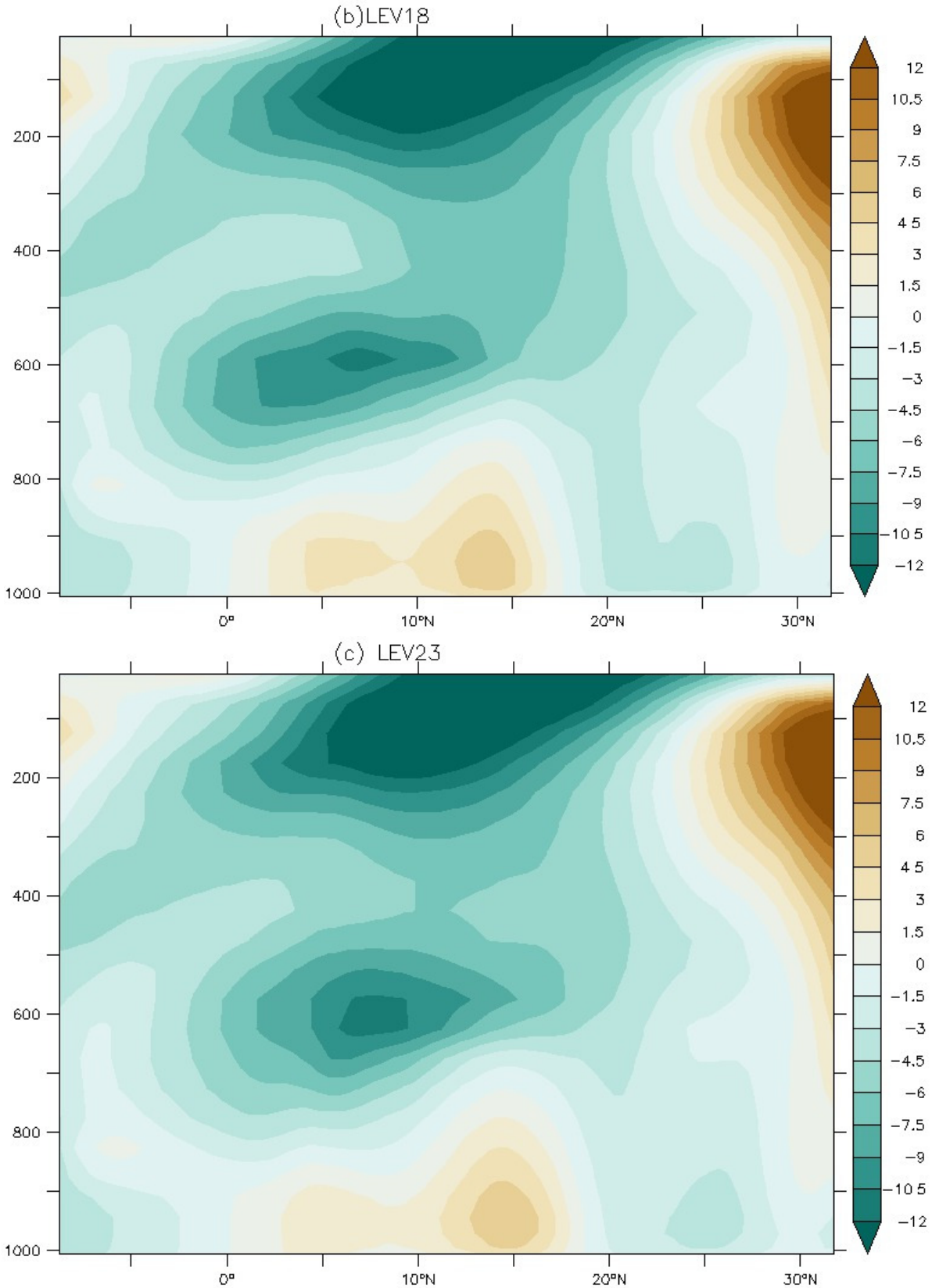

Figure-8: JJA zonal average of uwind (ms^{-1}) from (a) Era-Interim, (b) LEV18 and (c) LEV23 experiments in 2007. The uwind is averaged over 15°W to 15°E.

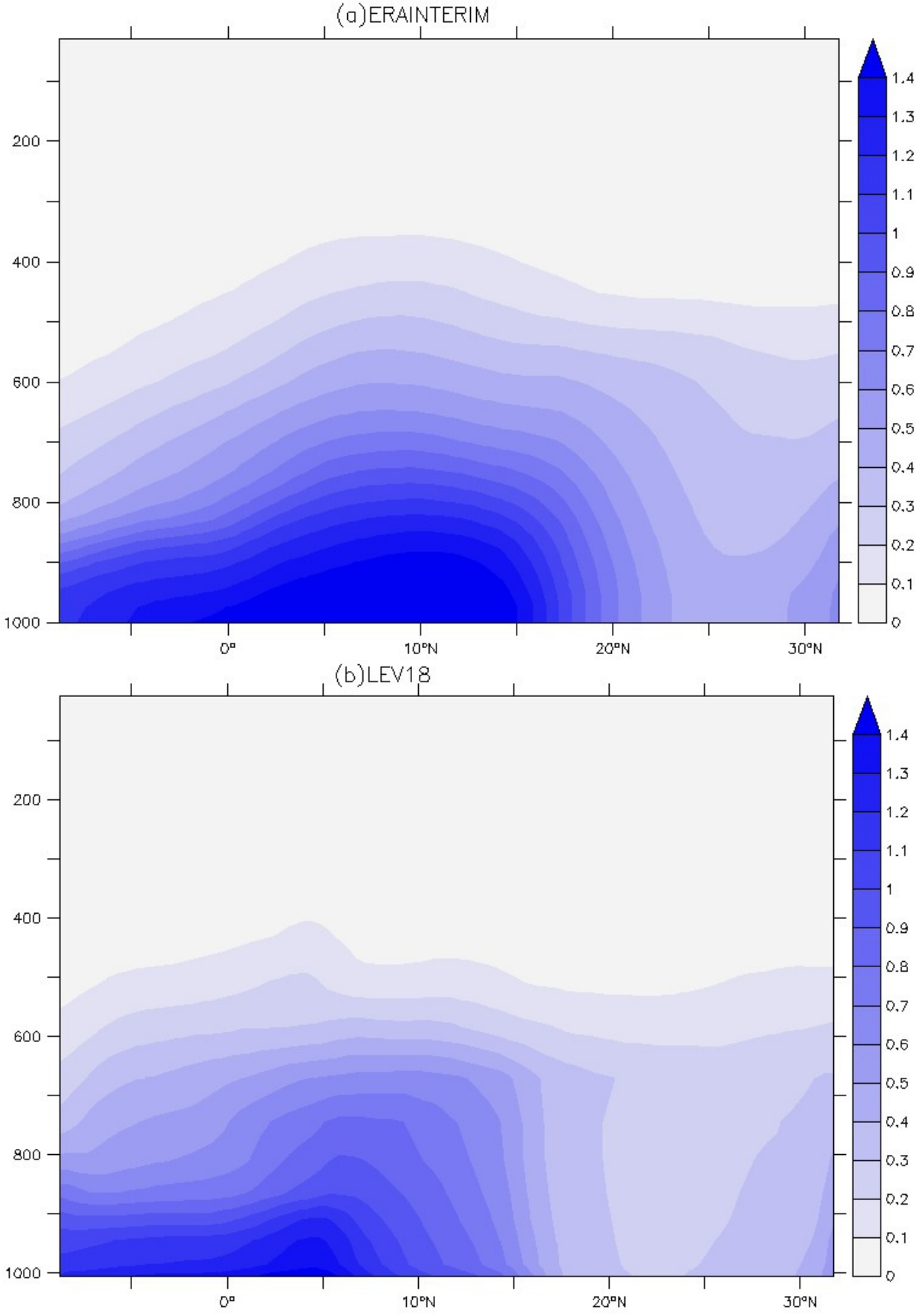
(a)ERAINTERIM
200
400
600
800
1000
0°
10°N
20°N
30°N
1.4
1.3
1.2
1.1
1
0.9
0.8
0.7
0.6
0.5
0.4
0.3
0.2
0.1
0
(b)LEV18
200
400
600
800
1000
0°
10°N
20°N
30°N
1.4
1.3
1.2
1.1
1
0.9
0.8
0.7
0.6
0.5
0.4
0.3
0.2
0.1
0

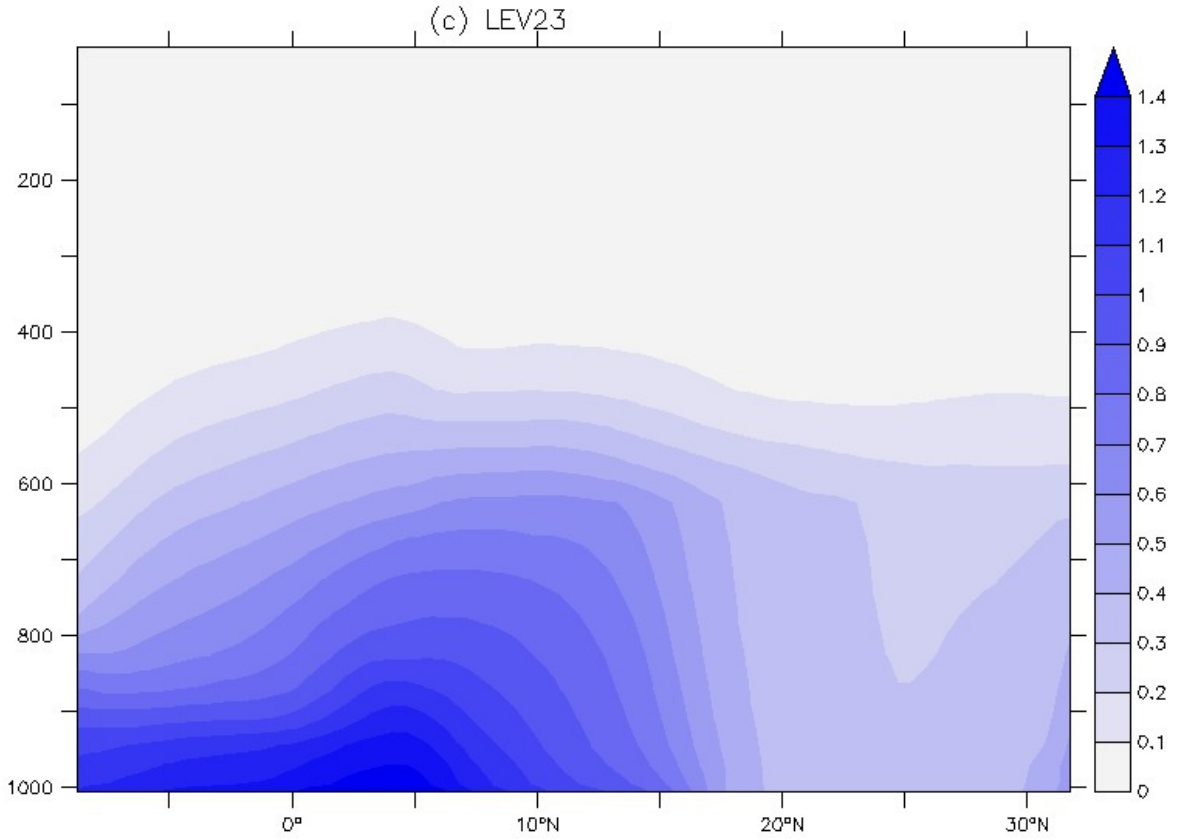

Figure-9: JJA zonal average of specific humidity(x 10^{-2} $kgkg^{-1}$) from (a) Era-Interim, (b) LEV18 and (c) LEV23 experiments. Specific humidity is averaged over 15°W to 15°E.

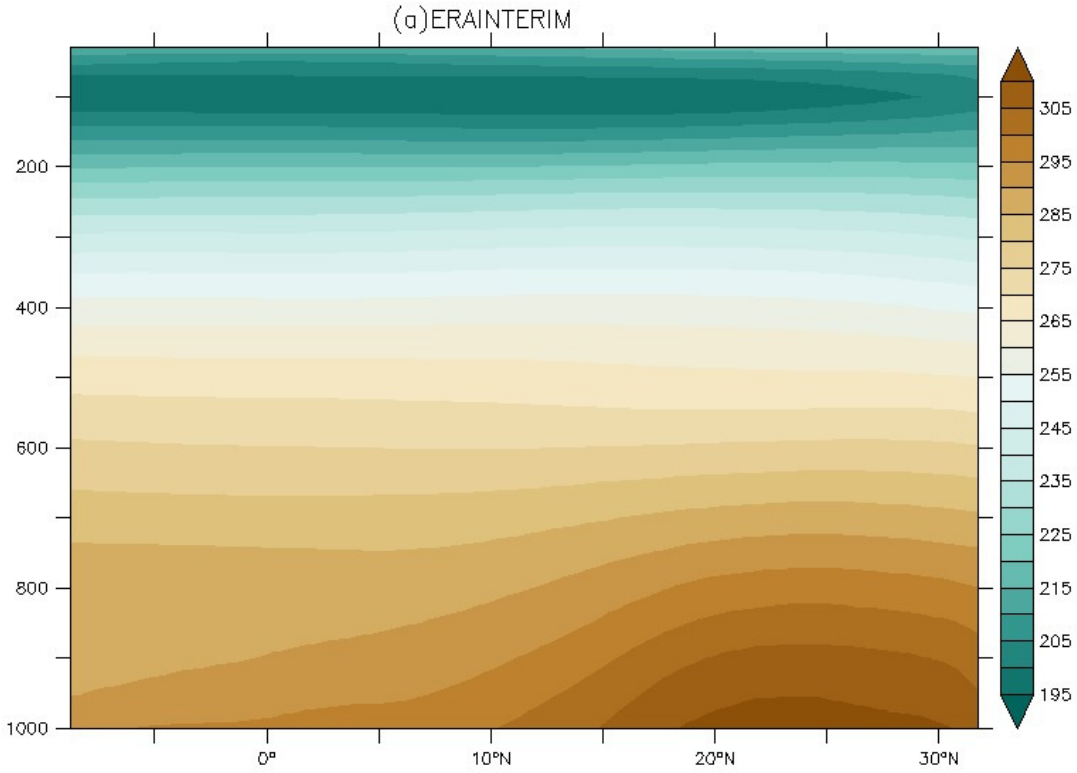

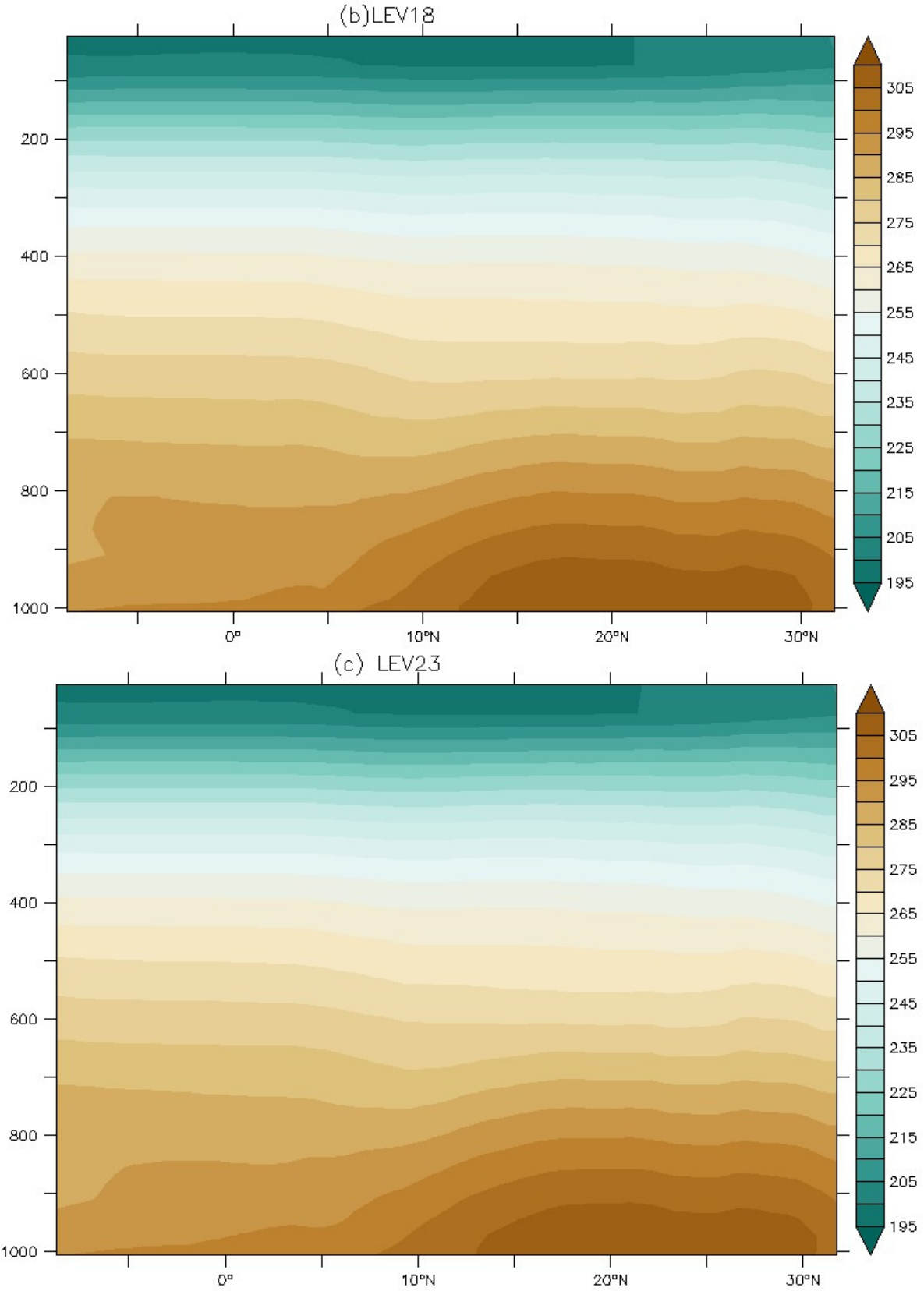

Figure-10: JJA zonal average of temperature (K) from (a) Era-Interim, (b) LEV18 and (c) LEV23 experiments in 2007. Temperature is averaged over 15°W to 15°E.

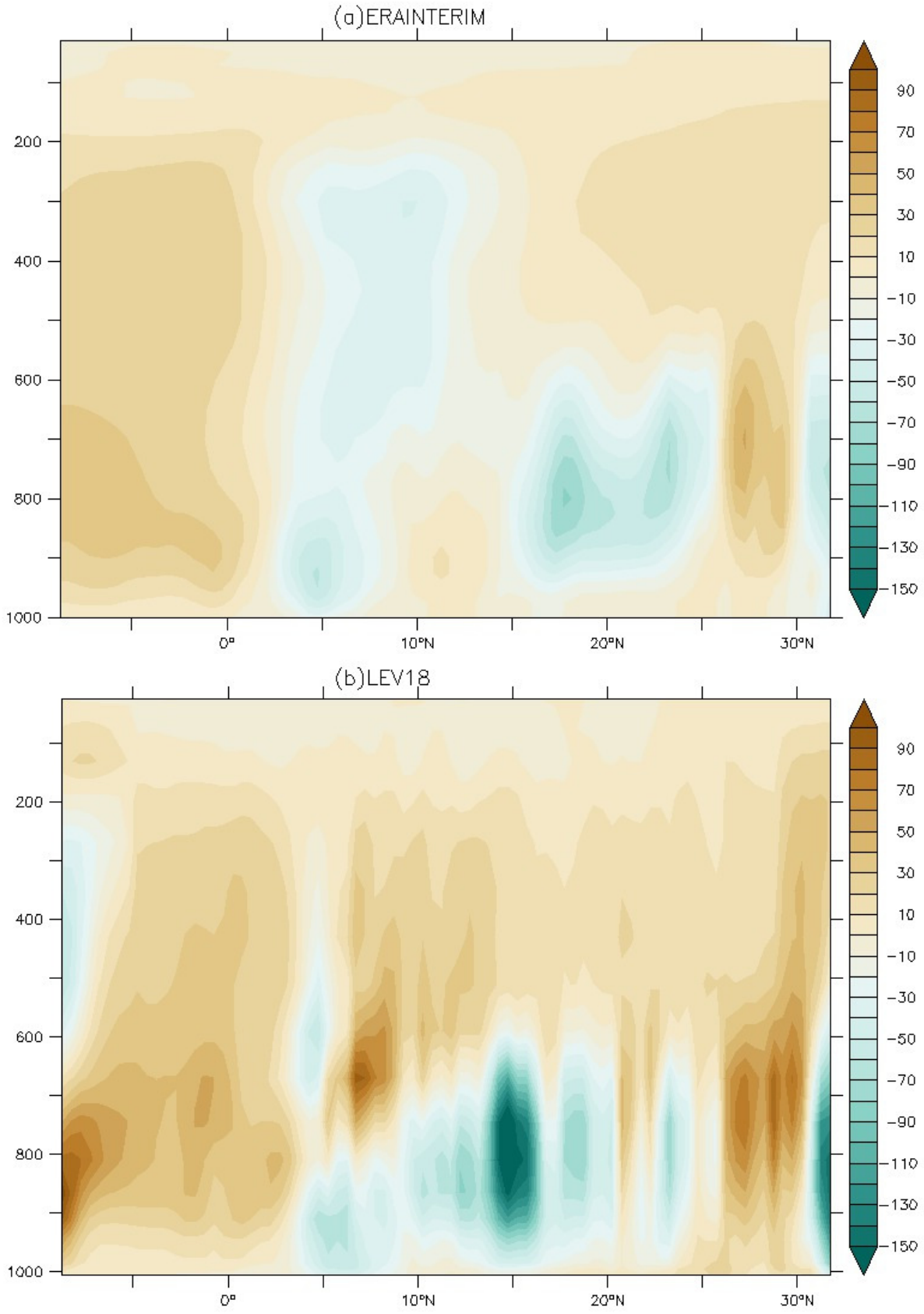
(a)ERAINTERIM
200
400
600
800
1000
0°
10°N
20°N
30°N
90
70
50
30
10
−10
−30
−50
−70
−90
−110
−130
−150
(b)LEV18
200
400
600
800
1000
0°
10°N
20°N
30°N
90
70
50
30
10
−10
−30
−50
−70
−90
−110
−130
−150

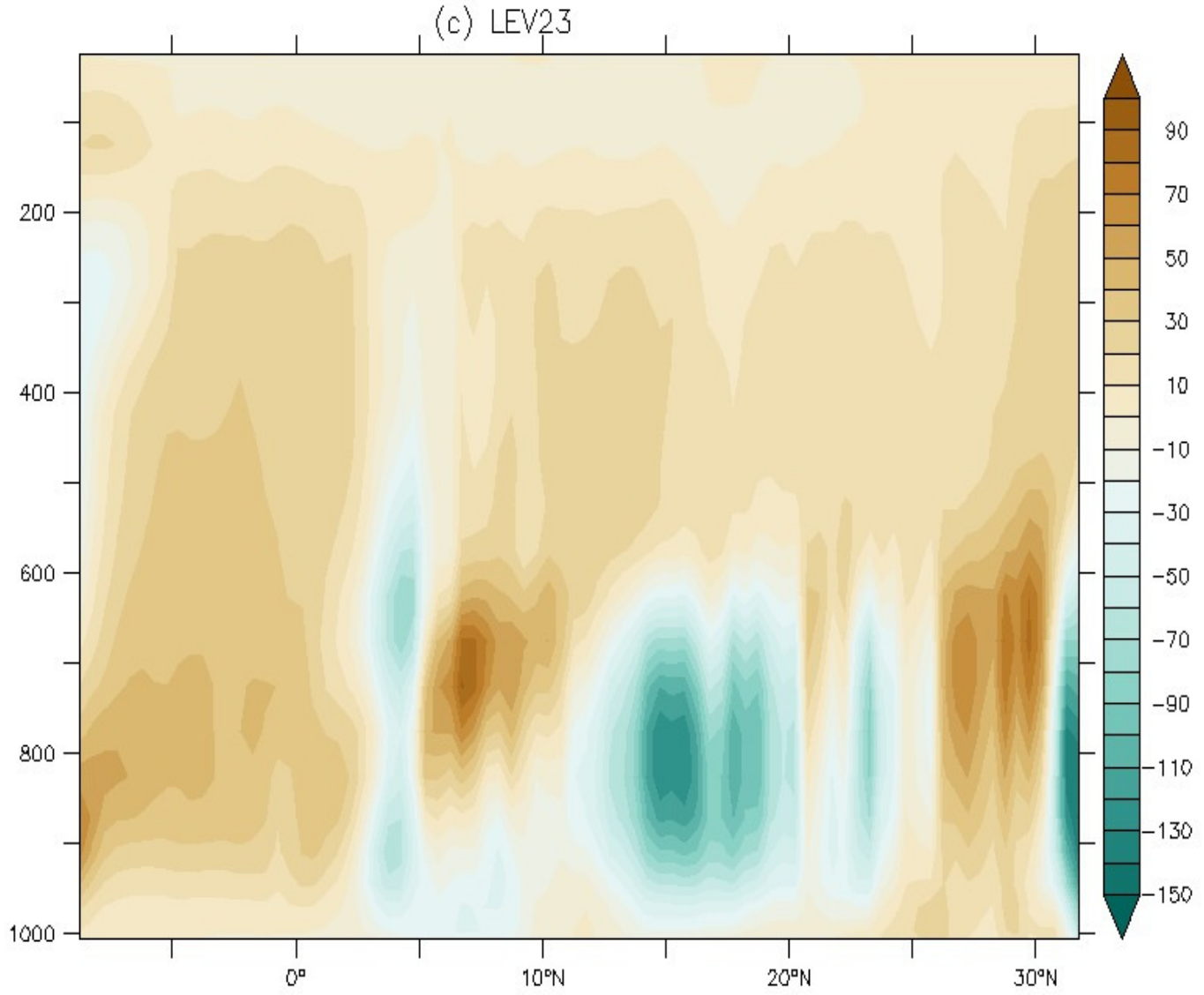

Figure-11: JJA zonal average of omega pressure velocity (x 10^{-5} $hPas^{-1}$) from (a) Era-Interim, (b) LEV18 and (c) LEV23 experiments in 2007. Omega pressure velocity is averaged over 15°W to 15°E.

Validation of simulated Radiation heating rate: Cross-section of simulated Shortwave Radiation Heating rate (QRS) at 0°E for LEV18 and LEV23 is shown in Figure-12. Higher vertical and north-south spread of high QRS is simulated in LEV23 at the mid-troposphere but lower heating rate at the surface compared to LEV18. The shortwave heating rate is conspicuous at 5-10°N from the surface to the mid-troposphere. Figure-13 shows the crossection of simulated Longwave Radiation Heating Rate (QRL) at 0°E for LEV18 and LEV23.Magnitude of QRL is highest at the mid-troposphere and lowest at 200-100 hPa.

The vertical profile of QRL is similar to that of QRS (Figure-12 and 13). The greenhouse gases, including tropospheric ozone contributes to the highest magnitude of radiation heating rate at the mid-troposphere. Figure-14 shows simulated Surface Net Downward Shortwave (RSNS) in LEV18 and LEV23. LEV23 shows wide spread low values (RSNS < 195 Wm^{-2} below 12°N on land). Whereas such values are scanty in LEV18.

Simulated Surface Net Downward Longwave (RSNL) in LEV18 and LEV23 is shown in Figure-15. RSNL values less than 70 Wm^{-2} is wide spread over land and ocean at the south below 15°N in LEV23 but scanty in LEV18 (Figure-15a, b). Lowest values are located at the mountains. The RSNS and RSNL have the same spatial variation but RSNL values are lower as expected. The albedo of the various surfaces such as water, mountain, soil colour and desert, to mention a few affects the downward shortwave radiation and upward longwave radiation. Surfaces with low albedo such as lakes, oceans and forests have high RSNS and RSNL while surfaces with high albedo such as desert snow on mountains and sea ice have low RSNS and RSNL.

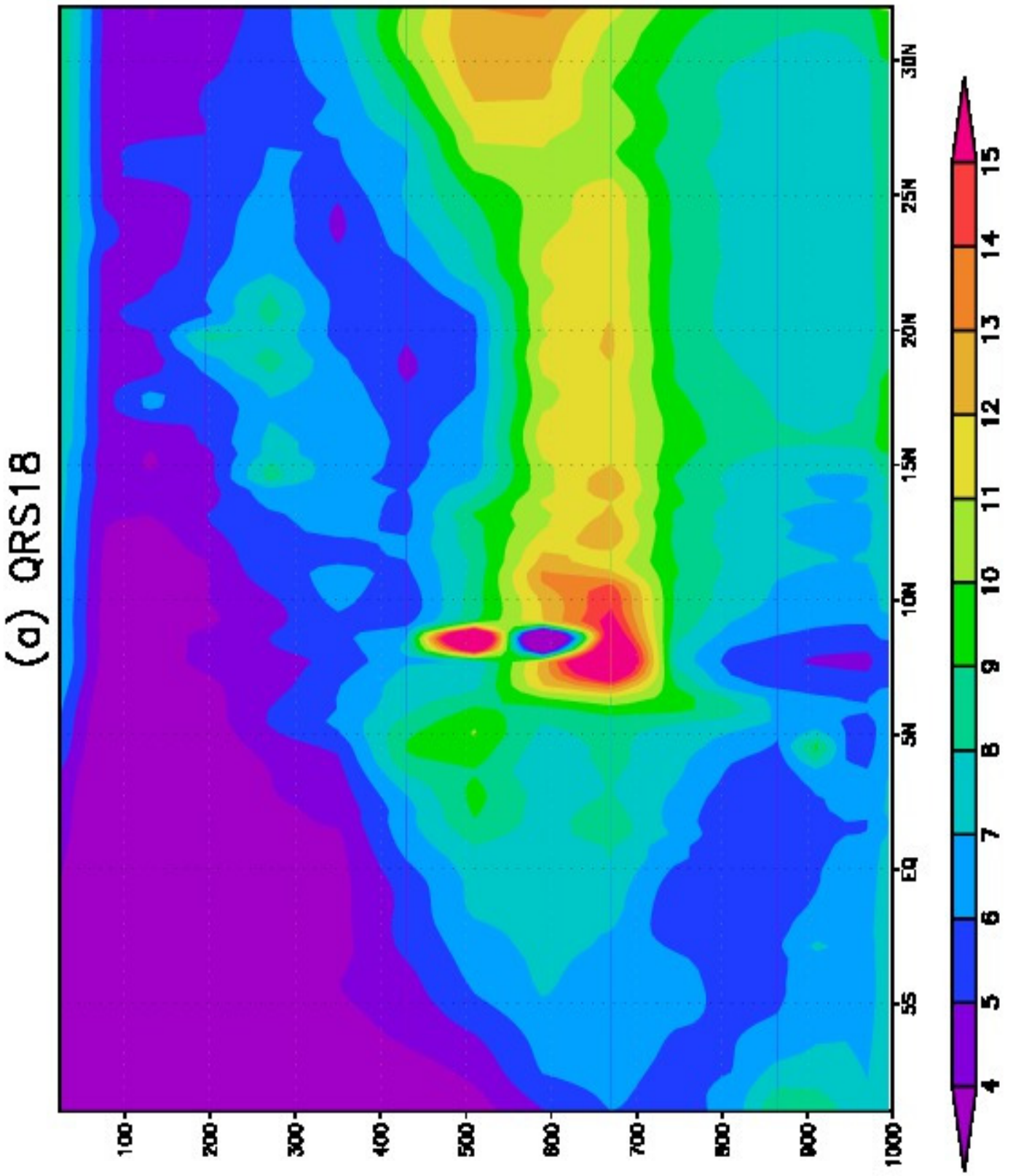
(a) QRS18
100
200
300
400
500
600
700
800
900
1000
55
EQ
5N
10N
15N
20N
25N
30N
4
5
6
7
8
9
10
11
12
13
14
15

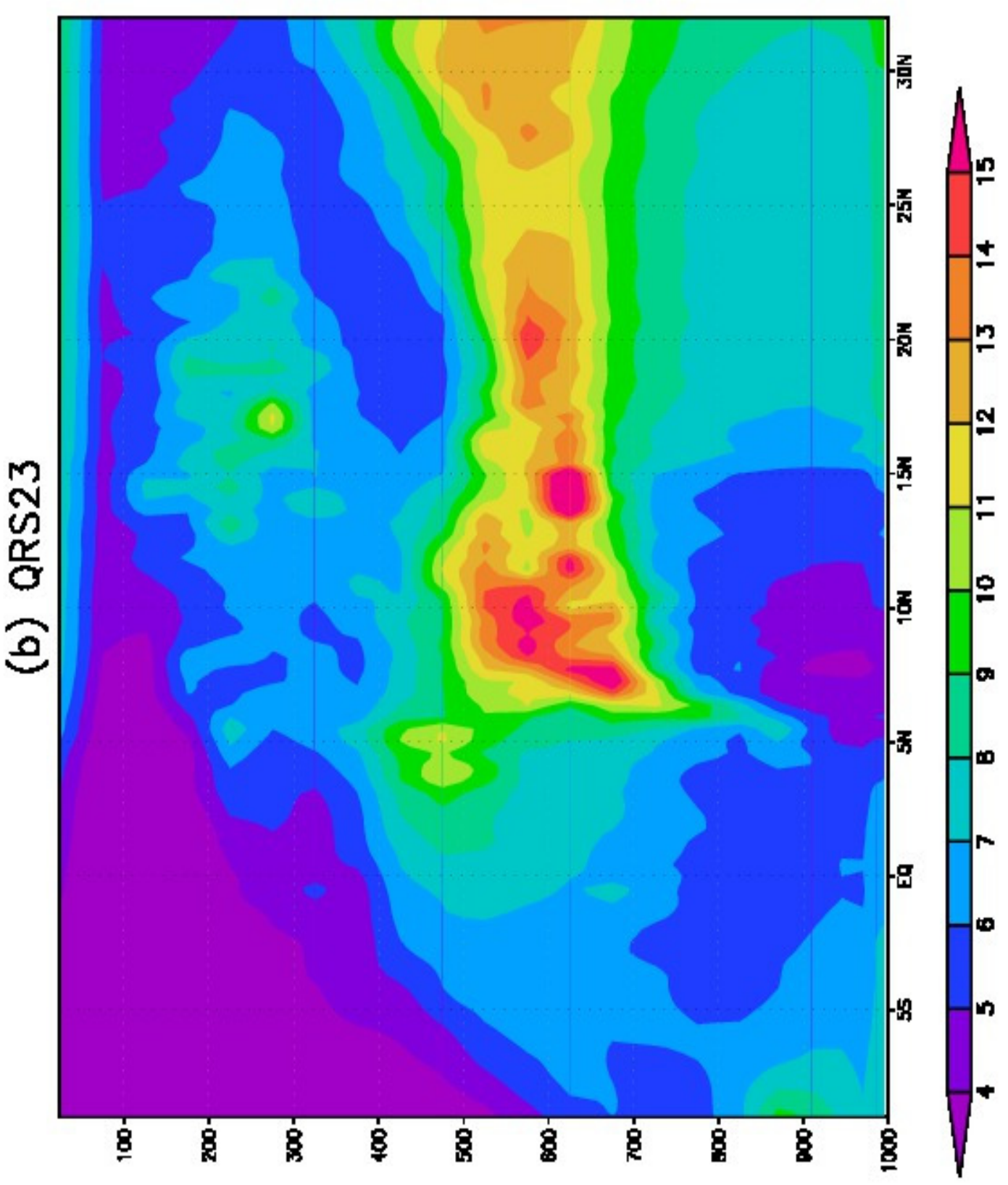

Figure-12: Cross-section of 0°E mean July shortwave radiation heating rate (x 10^{-6} Ks^{-1}) for (a) LEV18 experiment and (b) LEV23 experiment in 2007.

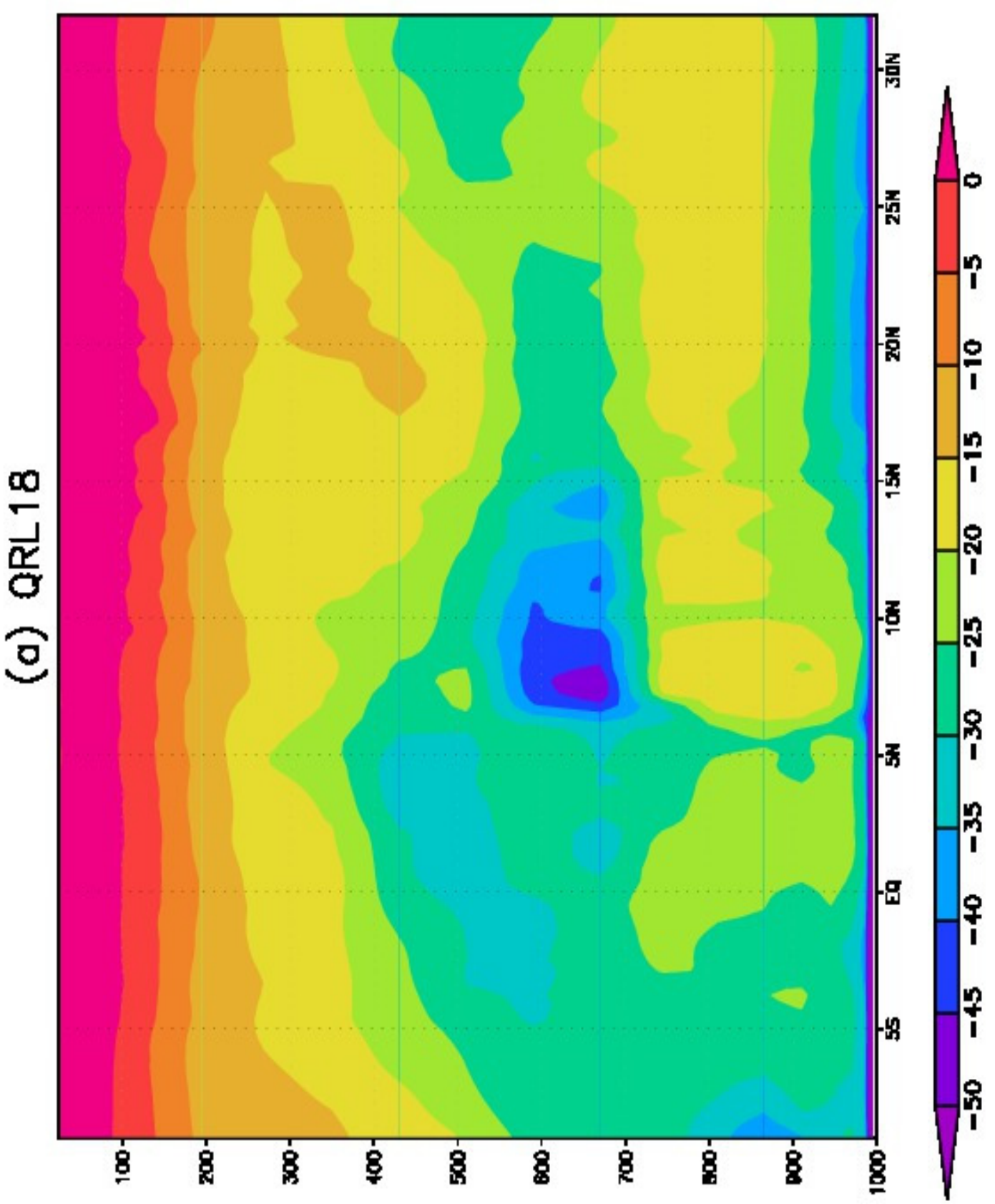
(a) QRL18
100
200
300
400
500
600
700
800
900
1000
55
EQ
5N
10N
15N
20N
25N
30N
0
-5
-10
-15
-20
-25
-30
-35
-40
-45
-50

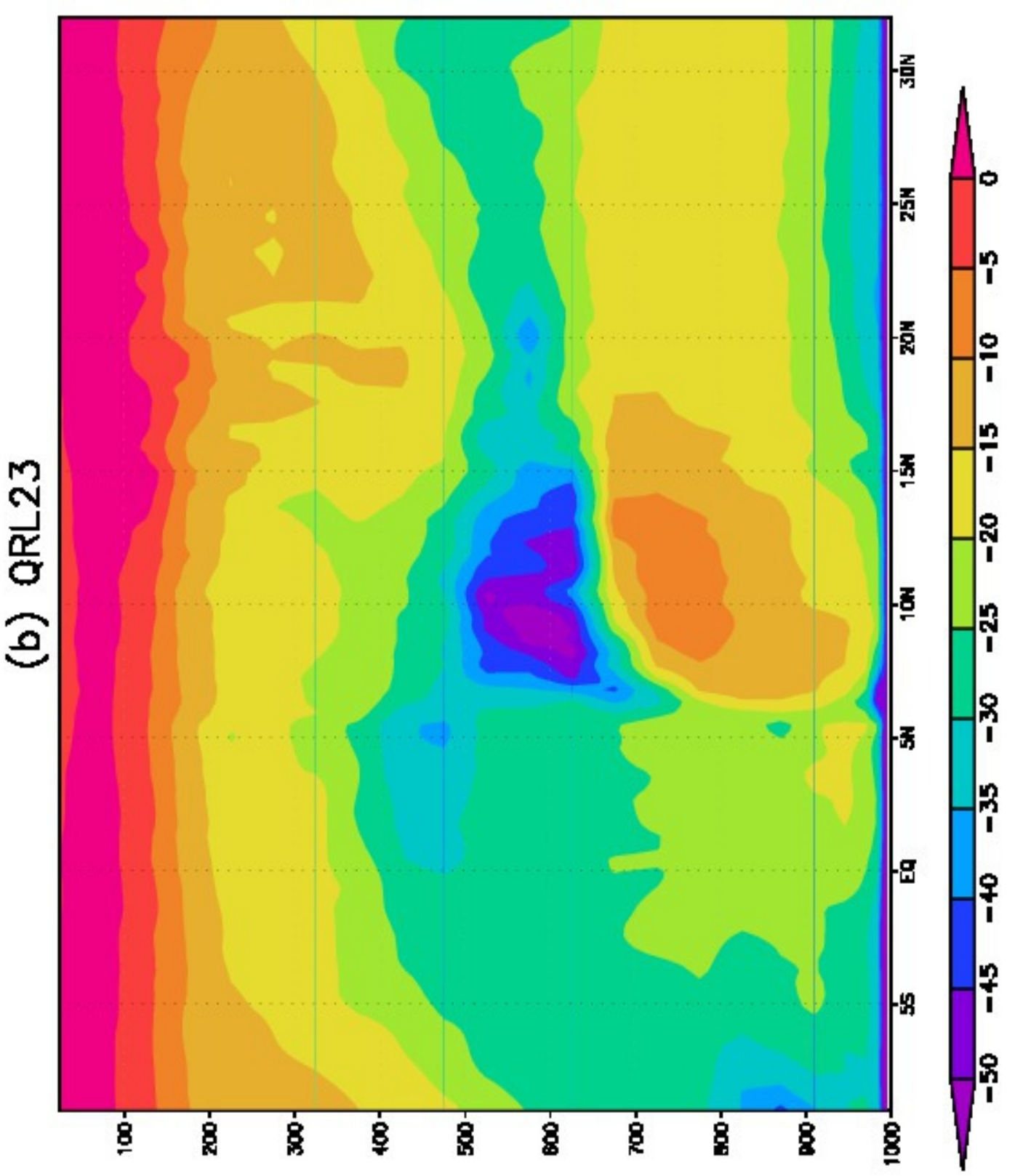

Figure-13: Cross-section of 0°E mean July longwave radiation heating rate (x 10^{-6} Ks^{-1}) for (a) LEV18 experiment and (b) LEV23 experiment in 2007.

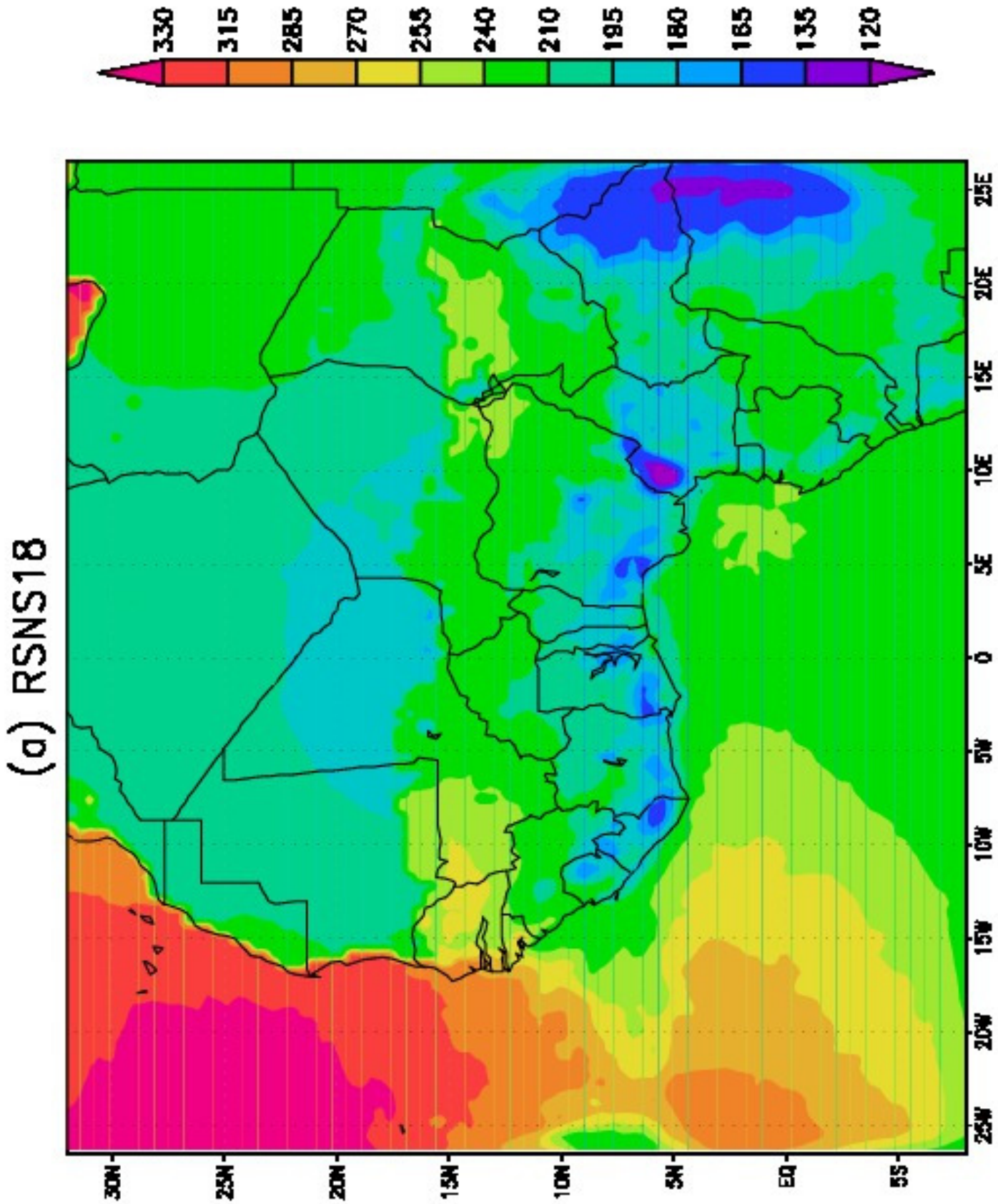
330
315
285
270
255
240
210
195
180
165
135
120
(a) RSNS18
30N
25N
20N
15N
10N
5N
EQ
5S
25W
20W
15W
10W
5W
0
5E
10E
15E
20E
25E

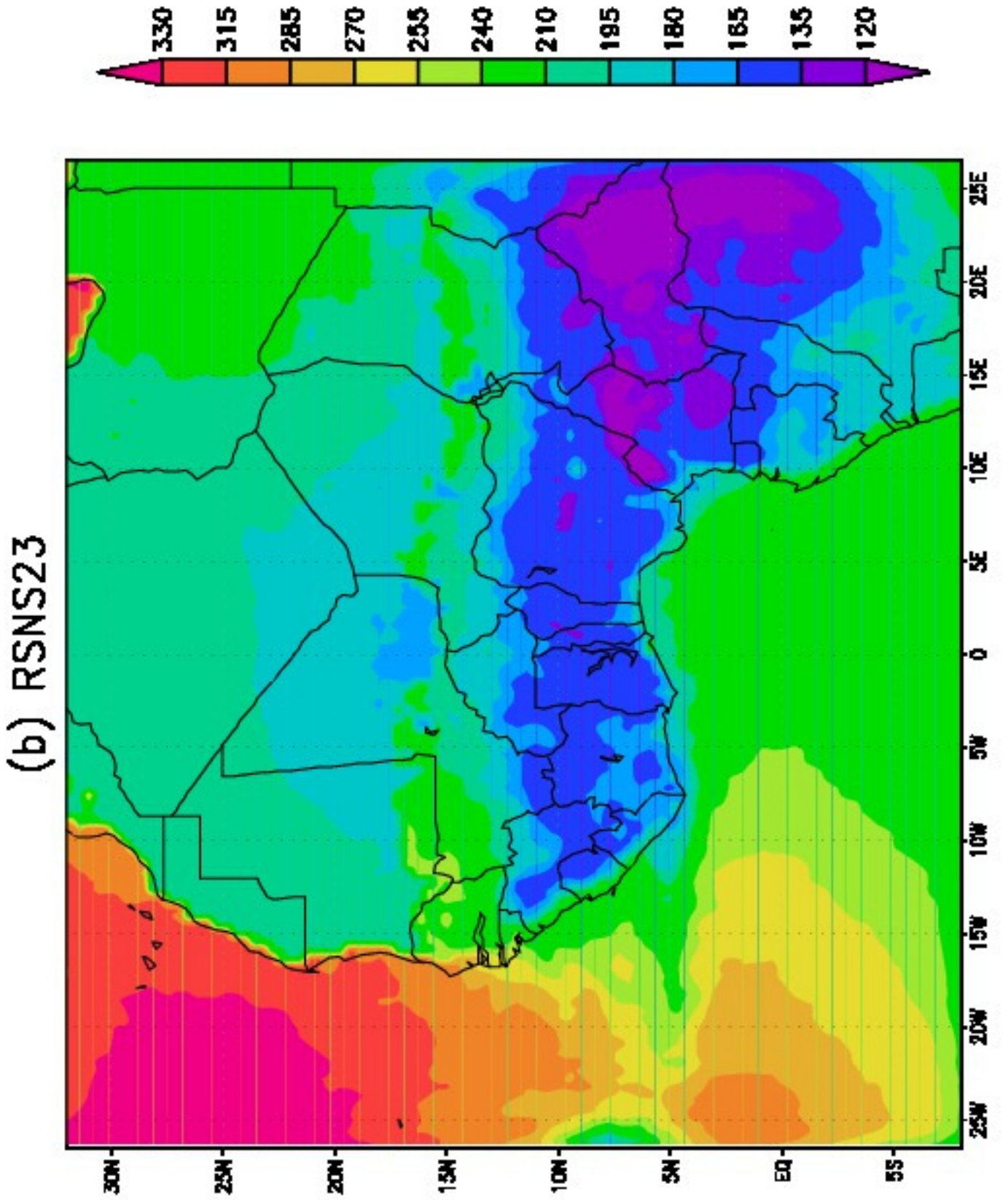

Figure-14: JJA surface net downward shortwave radiation (Wm^{-2}) from (a) LEV18 experiment and (b) LEV23 experiment in 2007.

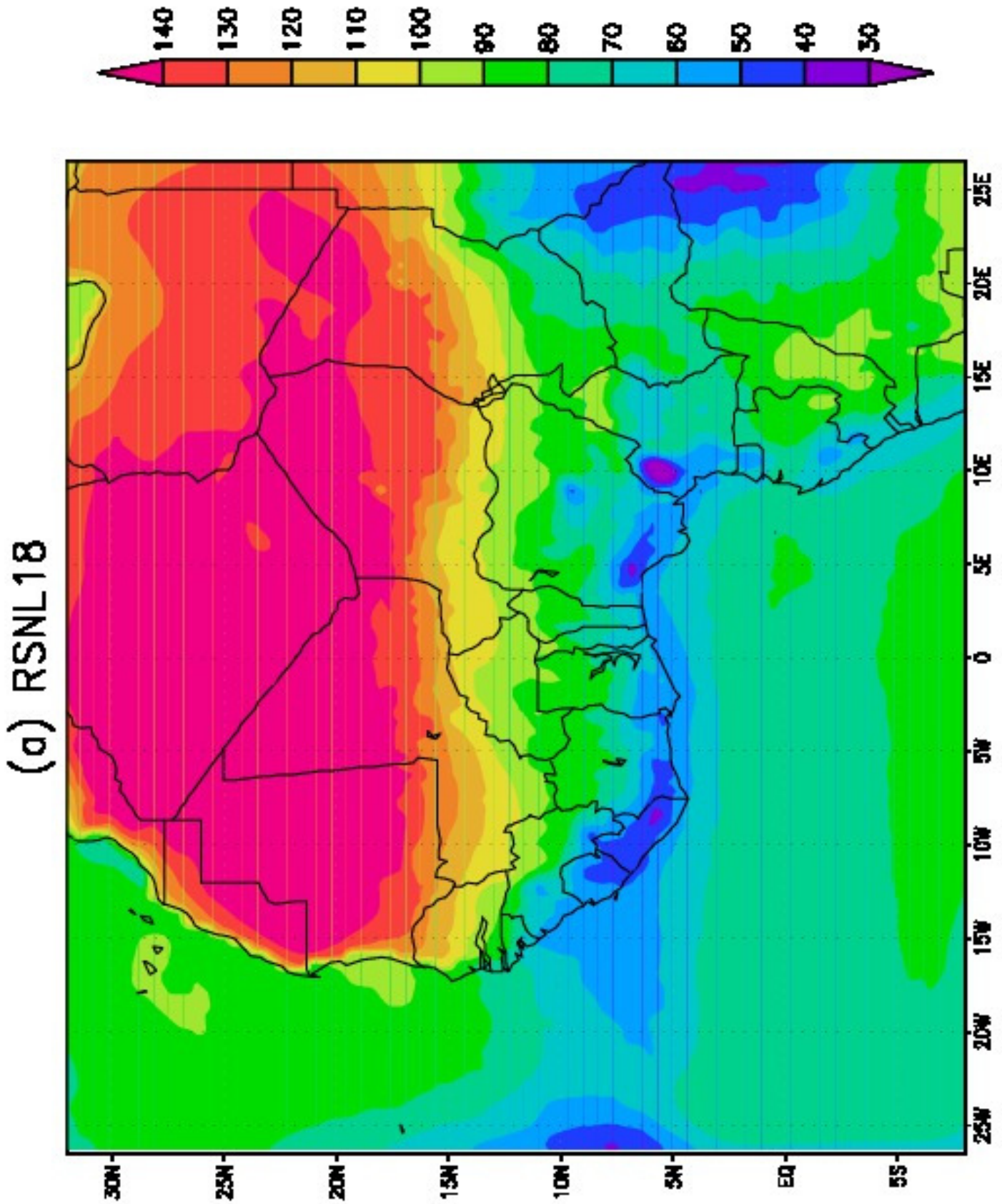
140
130
120
110
100
90
80
70
60
50
40
30
(a) RSNL18
30N
25N
20N
15N
10N
5N
EQ
5S
25W
20W
15W
10W
5W
0
5E
10E
15E
20E
25E

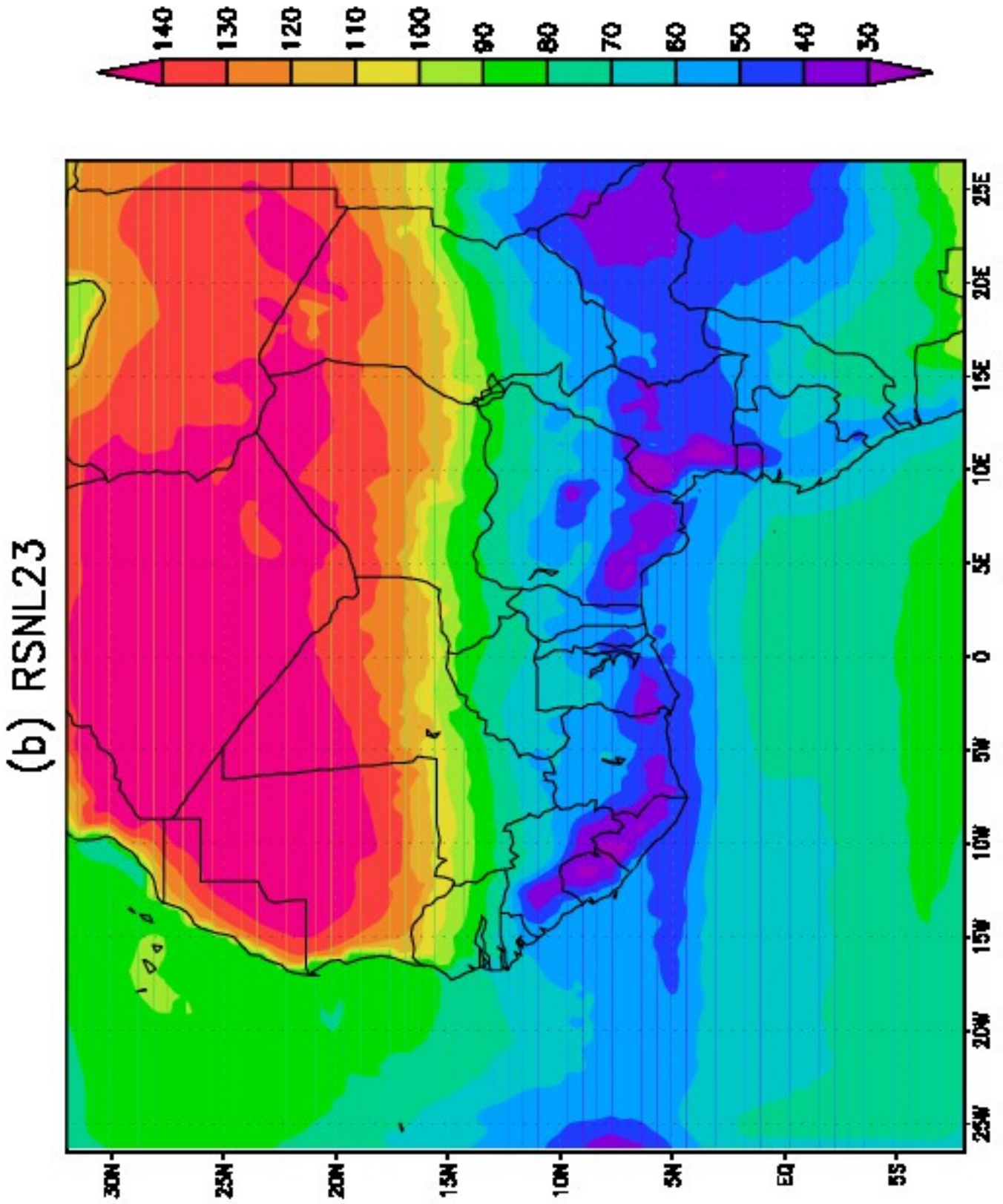

Figure-15: JJA surface net upward longwave radiation flux (Wm^{-2}) from (a) LEV18 experiment and (b) LEV23 experiment in 2007.

Conclusion

Influence increased resolution in the vertical on climate is simulated with RegCM4.5 based on 18 and 23 number of vertical levels (LEV18 and LEV23). This was tested over West Africa. The two different model levels are different from the surface up to the upper troposphere but the levels are the same from 150 hPa to the pressure top of the model. A similar set-up was used in ECHAM4 with more vertical model layers at the upper troposphere[16]. They reported improved performance of convective precipitation parameterization schemes with the increased vertical resolution. In this work, LEV23 simulates more realistic precipitation than LEV18 with respect to observed CRU and GPCP. Observed NOAA deep convection (OLR < 245 Wm^{-2}) in southern part of the simulation domain is wide spread. Simulated deep convection in LEV23 has similar spatial structure with NOAA while only a few isolated areas have deep convection in LEV18. Both LEV18 and LEV23 experiments underestimate ground temperature at the northern part of the simulation domain and overestimate it at the southern part of the domain. However, LEV23 simulates ground temperature with lower bias than LEV18 with respect to Era-Interim reanalysis. Convective precipitation dominates West Africa[29]. Also, higher proportion of convective precipitation is simulated by higher vertical resolution in ECHAM4 model[16]. The LEV23 experiment simulates greater proportion of convective precipitation below 15^{o}N as expected. LEV23 resolves cloud water content up to 500 hPa as observed in Era-Interim. The simulated cloud water content in LEV23 is more realistic than in LEV18. This corroborates previous reports[13,16]. Strength of AEJ simulated in LEV23 is more comparable to Era-Interim, LEV23 experiment also resolves specific humidity better at the north with respect to Era-Interim reanalysis. Furthermore, the vertical extent of specific humidity is better captured by LEV23 than LEV18. Both LEV18 and LEV23 experiments resolve air temperature well at the upper and mid troposphere, but LEV23 resolves air temperature better at the lower troposphere. Influence of greenhouse gases including tropospheric ozone on radiation heating rate in the vicinity of the mid-troposphere is better resolved in LEV23 experiments. Omega pressure velocity is captured with lower N-S extent and differing strengths in LEV18 and LEV23 simulations with respect to Era-Interim reanalysis. Albedo effect on surface net radiation is better resolved by LEV23 experiment. The results show better resolved climate with increased vertical resolution using the same horizontal resolution.

Acknowledgements

The author is forever grateful to the climate modelling research group at ICTP for releasing the RegCM4.5 used in this investigation. Climate Research Unit of the University of East Anglia time series and GPCP data were used. National Oceanic and Atmospheric Administration (NOAA) provided the OLR satellite retrieved data and the Era-Interim reanalysis datasets used were obtained from ECMWRF.

References

1. Williams J.J., Esteves L.S. and Rochford L.A. (2015). Modelling storm responses on a high energy coastline with XBeach. *Model. Earth Syst. Environ.,* 1(1-2), 3.

2. Yospin G.I., Wood S.W., Holz A., Boeman D.M., Keane R.E. and Whitlock C. (2015). Modelling vegetation mosaics in sub-alpine Tasmania under various fire regimes. *Model Earth Syst. Environ.,* 1(3), 16.

3. Das Y., Mohanty U.C. and Jain I. (2016). Development of tropical cyclone wind field for simulation of storm surge/sea surface height using numerical ocean model. *Modeling Earth Systems and Environment*, 2(1), 13.

4. Shrivastava S., Bal P.K., Ashrit R., Sharma K., Lodh A. and Mitra A.K. (2017). Performance of NCUM global weather modeling system in predicting the extreme rainfall events over the central India during the Indian summer monsoon 2016. *Modeling Earth Systems and Environment*, 3(4), 1409-1419. http://doi.org/10.1007/s408001703878.

5. Jisan M.A., Bao S., Pietrafesa L.J., Shen D., Gayes P.T. and Hallstrom J. (2018). Hurricane Matthew (2016) and its impact under global warming scenarios. *Modeling Earth Systems and Environment*, 4(1), 97-109. https://doi.org/10.1007/s40808-018-0420-6.

6. Brown C., Greene A., Block P. and Giannini A. (2008). Review of Downscaling Methodologies for Africa Climate Applications. IRI Technical Report 08 – 05, IRI Downscaling Report. International Reasearch Institute for Climate and Society. Columbia University.

7. Jones C., Giorgi F. and Asrar G. (2011). The Coordinated Regional Downscaling Experiment: CORDEX An international downscaling link to CMIP5. *CLIVAR Exchanges,* 56(16), 34-41.

8. Nikulin G., Jones C., Giorgi F., Asrar G., Buchner M., Cerezo-mota R., Christensen O.B., DeQue M., Fernandez J., Hansler A., Meijgaard E.V., Samuelsson P., Sylla M.B. and Sushama L. (2012). Precipitation climatology in an ensemble of CORDEX-Africa regional climate simulations. *J. Clim.,* 25, 6057-6078.

9. Liess S. and Bengtsson L. (2004). The intraseasonal oscillation in ECHAM4 Part II: sensitivity studies. *Climate dynamics*, 22(6-7), 671-688.

10. Land C., Ponater M., Sausen R. and Roeckner E. (1999). The ECHAM4. L39 (DLR) atmosphere GCM – Technical description and model climatology. *DLR Forschungsbericht*, 1999-31, 45. ISSN 1434-8454, Deutsches Zentrum fur Luft- und Raumfahrte, 51170 Koln, Germany.

11. Roeckner E., Brokopf R., Esch M., Giorgetta M., Hagemann S., Kornblueh L., Manzini E., Schlese U. and Schulzweida U. (2004). The atmospheric general circulation model ECHAM 5. PART II: Sensitivity of

Simulated Climateto Horizontal and Vertical Resolution, MPI-Report 354, 56. (mpi_report_354.pdf, 10.7 MB).

12. Lindzen R.S. and Fox-Rabinovitz M. (1989). Consistent vertical and horizontal resolution. *Monthly Weather Review*, 117(11), 2575-2583.

13. Inness P.M., Slingo J.M., Woolnough S.J., Neale R.B. and Pope V.D. (2001). Organization of tropical convection in a GCM with varying vertical resolution; implications for the simulation of the Madden-Julian Oscillation. *Climate Dynamics*, 17(10), 777-793.

14. Pope V.D., Pamment J.A., Jackson D.R. and Slingo A. (2001). The representation of water vapor and its dependence on vertical resolution in the Hadley Centre Climate Model. *Journal of climate*, 14(14), 3065-3085.

15. Spencer H. and Slingo J.M. (2003). The simulation of peak and delayed ENSO teleconnections. *J. Clim.,* 16(11), 1757-1774.

16. Ruti P.M., Rocco D.D. and Gualdi S. (2006). Impact of increased vertical resolution on simulation of tropical climate. *Theor. Appl. Climatol.*, 85(1-2), 61-80.

17. Tang J.P., Zhao M. and Su B.K. (2007). The effects of model resolution on the simulation of regional climate extreme events. *Acta Meteorologica Sinica,* 21(2), 129-140.

18. Druyan L.M., Fulakeza M. and Lonergan P. (2008). The impact of vertical resolution on regional model simulation of the West African summer monsoon. *International Journal of Climatology*, 28(10), 1293-1314.

19. Zeng X., Wang M., Zhang Y., Wang Y. and Zheng Y. (2016). Assessing the Effects of Spatial Resolution on Regional Climate Model Simulated Summer Temperature and Precipitation in China: A Case Study. *Advances in Meteorology*. ID 7639567: 12 pages.http://dx.doi.org/10.1155/2016/7639567.

20. Elguindi N., Bi X., Giorgi F., Nagarajan B., Pal J., Solmon F., Rauscher S., Zakey A., O'Brien T., Nogherotto R. and Giulian G. (2014). Regional climate model user's manual version 4.4. Earth system physics section. *The Abdus Salam International Centre for Theoretical Physics*, Trieste.

21. Giorgi F., Coppola E., Solmon F., Mariotti L., Sylla M.B., Bi X., Elguindi N., Diro G.T., Nair V., Giuliani G., Turuncoglu U.U., Cozzini S., Gu¨ttler I., O'Brien T.A., Tawfik A.B., Shalaby A., Zakey A.S., Steiner A.L., Storda F., Sloan L.C. and Brankovic C. (2012). RegCM4 model description and preliminary tests over multiple CORDEX domains. *Climate Research*, 52, 7-29.

22. Giorgi F., Solmon F. and Giuliani G. (2016). Regional Climatic Model RegCM User's Guide Version 4.5 Trieste, Italy.

23. Adeniyi M.O. (2014). Sensitivity of different convection schemes in RegCM4.0 for simulation of precipitation during the Septembers of 1989 and 1998 over West Africa. *Theor. Appl. Climatol.*, 115(1-2), 305-322.

24. Mitchell T.D. and Jones P.D. (2005). An improved method of constructing a database of monthly climate observations and associated high-resolution grids. *International journal of climatology*, 25(6), 693-712.

25. Huffman G.J., Alder R.F., Morrissey M., Bolvin D., Curtis S., Joyce R., McGavock B. and Susskind J. (2001). Global precipitation at one degree daily resolution from multi-satellite observations. *Journal of Hydrometeorology,* 2, 36-50.

26. Yin X., Gruber A. and Arkin P. (2004). Comparison of the GPCP and CMAP merged gauge–satellite monthly precipitation products for the period 1979-2001. *Journal of Hydrometeorology*, 5(6), 1207-1222.

27. Bolvin D.T., Adler R.F., Huffman G.J., Nelkin E.J. and Poutiainen J.P. (2009). Comparison of GPCP monthly and daily precipitation estimates with high-latitude gauge observations. *Journal of Applied Meteorology and Climatology*, 48(9), 1843-1857.

28. Liebmann B. and Smith C.A. (1996). Description of a complete (interpolated) outgoing longwave radiation dataset. *Bulletin of the American Meteorological Society*, 77(6), 1275-1277.

29. Schumacher C. and Houze Jr, R.A. (2003). Stratiform rain in the tropics as seen by the TRMM precipitation radar. *Journal of Climate*, 16(11), 1739-1756.